Sensitivity and resolution of tomographic pumping tests in an alluvial aquifer

Geoffrey C. Bohling[1]

Received 27 June 2008; revised 28 November 2008; accepted 17 December 2008; published 14 February 2009.

[1] Various investigators have proposed hydraulic tomography, the simultaneous analysis of responses to multiple well tests, as a means to obtain a high-resolution characterization of aquifer flow properties. This study assesses the information content of drawdown records from a set of tomographic pumping tests in an alluvial aquifer, comparing the parameter sensitivity and resolution associated with transient and steady-shape formulations of the objective function for the parameter estimation problem. The steady-shape approach takes advantage of the rapid establishment of constant gradients within the region surrounding a pumping well, comparing observed drawdown differences within this region with drawdown differences predicted by a steady state model. Both the transient and steady-shape approaches resolve K variations only within a limited distance of the pumping intervals and observation points. Relative to the transient approach, the steady-shape approach reduces the influence of poorly resolved property variations, including K variations outside the region of investigation and storage coefficient variations throughout the model domain.

Citation: Bohling, G. C. (2009), Sensitivity and resolution of tomographic pumping tests in an alluvial aquifer, *Water Resour. Res.*, *45*, W02420, doi:10.1029/2008WR007249.

1. Introduction

[2] Various studies have indicated the need for higher-resolution depictions of aquifer property variations than can be obtained from traditional aquifer characterization techniques. While the relatively large-scale average estimates of hydraulic conductivity (K) and specific storage (S_s) provided by traditional pumping test analysis will often suffice for water supply investigations, a number of studies have indicated that detailed characterization of the K distribution will often be required for accurate prediction of contaminant transport in the subsurface [*Gelhar and Axness*, 1983; *Sudicky*, 1986; *Dagan*, 1989; *Boggs et al.*, 1992; *Koltermann and Gorelick*, 1996; *Dagan and Neuman*, 1997; *Zheng and Gorelick*, 2003]. Various investigators [*Neuman*, 1987; *Tosaka et al.*, 1993; *Bohling*, 1993; *Gottlieb and Dietrich*, 1995; *Butler et al.*, 1999; *Yeh and Liu*, 2000; *Vesselinov et al.*, 2001a, 2001b; *Bohling et al.*, 2002; *Liu et al.*, 2002; *Brauchler et al.*, 2003; *Zhu and Yeh*, 2005; *Liu et al.*, 2007; *Bohling et al.*, 2007; *Straface et al.*, 2007; *Illman et al.*, 2007, 2008] have proposed hydraulic tomography, essentially the simultaneous analysis of responses to multiple stresses (pumping tests, etc.) as a means to reduce the nonuniqueness in estimates of the distribution of K and possibly also S_s. However, despite the allusion to geophysical methods through use of the term "tomography," we are still lacking in studies that take advantage of the tools used by geophysicists [*Menke*, 1989; *Aster et al.*, 2005; *Xia et al.*, 2008] to assess the resolution of our test designs.

[3] Following an approach suggested by *Vasco et al.* [1997], this study uses resolution matrices computed from first-order sensitivity (Jacobian) matrices to examine how well a set of tomographic pumping tests in an alluvial aquifer resolves the K and S_s variations in the vertical plane between the two pumping wells used in the tests. *Clemo et al.* [2003] used essentially the same approach to examine the ability of a single, fully penetrating pumping test with multiple observation wells to resolve areal variations in transmissivity. The observation well configuration for the simulations consisted of 12 observation wells distributed in two concentric rings around a central pumping well, with pumping/observation well separation distances of roughly 4 and 9 m, mimicking the configuration of the central well cluster at the Boise Hydrogeophysical Research Site [*Barrash and Reboulet*, 2004; *Barrash and Clemo*, 2002]. The results presented by *Clemo et al.* [2003] indicate that K variations can only be adequately resolved in a fairly limited region around the pumping well and in the immediate vicinity of the observation wells. Although *Clemo et al.* [2003] investigate the resolution for a single-well, constant-rate pumping test, rather than a set of tomographic pumping tests, their study can be taken to reflect the fundamental physics of radial flow tests. Indeed, the present study indicates that even with information obtained using multiple pumping/observation well configurations, resolution is focused on the pumping intervals and observation locations, with properties of materials at even moderate distances from these locations observable only in terms of bulk averages. Relative to the ambitious agenda implicit in the term "hydraulic tomography," these results are rather sobering. At the very least they indicate that the availability of an extensive suite of hydraulic data does not remove the need to regularize the inversion through incorporation of

[1]Kansas Geological Survey, University of Kansas, Lawrence, Kansas, USA.

0043-1397/09/2008WR007249

objective function terms that penalize deviations from an a priori parameter model [*Carrerra and Neuman*, 1986; *Kitanidis*, 1995; *Doherty*, 2003; *Tonkin and Doherty*, 2005; *Fienen et al.*, 2008; *Bohling*, 2008] and/or condition the estimates to independent measurements of the hydraulic parameters [*Carrera et al.*, 2005; *Illman et al.*, 2008] or correlated secondary data, such as geophysical parameters [*Rubin and Hubbard*, 2005; *Caers*, 2005].

[4] The primary objective of the current study is to compare the sensitivity and resolution associated with transient and steady-shape approaches to the analysis of a set of tomographic pumping tests in an alluvial aquifer. The transient formulation involves an objective function that measures discrepancies between observed drawdowns and their simulated equivalents, drawn from a transient model. As described by *Bohling et al.* [2002], the steady-shape approach involves formulating the objective function in terms of differences in drawdown between different observation locations at common observation times, drawing the simulated equivalents of these differences from a steady state model rather than from a transient model. This approach exploits the rapid establishment of steady-shape or transient steady state [*Kruseman and de Ridder*, 1990] flow conditions observed in many constant-rate pumping tests; under these conditions, drawdown gradients in the vicinity of the pumping well have reached their final steady state values although the drawdowns themselves have not. As demonstrated by *Bohling et al.* [2002], a steady-shape approach greatly reduces the computation time required for inversion, compared with a transient formulation of the same problem, and reduces the influence of uncertainty in boundary conditions, compared wtih analyzing the drawdowns themselves with a steady state model. It should be noted that ''steady-shape analysis'' or ''steady-shape inversion'' does not refer to an inversion algorithm. Instead, it refers to a way of formulating the objective function employed in an inverse analysis. The resulting objective function could be minimized using any number of inversion algorithms.

[5] *Bohling et al.* [2007] presented both transient and steady-shape analyses of drawdown data from 23 tomographic pumping tests in an alluvial aquifer at a site in northeastern Kansas. That study presents estimated K profiles based on various layered zonations of the K field and examines the utility of information derived from a zero-offset cross-hole radar survey between the two pumping wells in developing the zonations. Here we examine the potential for the tomographic pumping test configuration to delineate K variations in both the vertical and lateral directions based on a first-order sensitivity and resolution analysis. We compare the sensitivity and resolution associated with transient analyses of drawdown records representing early time data (0 to 30 s) and longer-term data (0 to 300 s) for each test and steady-shape analysis of the differences in drawdown between different locations at common times over the 20–70 s time frame.

[6] The present study demonstrates that even with a transient analysis of drawdown records from multiple pumping tests, we cannot expect to resolve spatial variations in K outside the region encompassed by the pumping and observation wells (referred to hereinafter as the region of investigation, or ROI) and that it is very difficult to resolve S_s variations anywhere in the model domain, at least in high-diffusivity aquifers. Nevertheless, the drawdowns are sensitive to the bulk averages of these properties. In contrast, the sensitivity of the drawdown differences analyzed in the steady-shape approach is focused almost entirely on K within the ROI. The resolution analyses indicate that K variations within the ROI are the only parameter variations that can be adequately resolved using either a transient or a steady-shape approach. That is, a steady-shape analysis reduces the influence of those parameters whose variations are poorly resolved even when we perform a transient analysis, namely, K outside the ROI and S_s everywhere in the model domain.

2. Experimental Configuration

[7] The sensitivity and resolution analyses presented here reflect the experimental configuration and general aquifer characteristics for a set of tomographic pumping tests at the Kansas Geological Survey's Geohydrologic Experimental and Monitoring Site (GEMS), an extensively studied site in the Kansas River valley northeast of Lawrence, Kansas. *Butler* [2005] and *Zemansky and McElwee* [2005] provide summaries of much of the hydraulic characterization work at GEMS. The highly conductive alluvial aquifer at the site, consisting of about 10.5 m of sand and gravel, is overlain by approximately 11 m of silt and clay. The bulk average hydraulic conductivity of the aquifer is about 1.5×10^{-3} m/s [*Butler*, 2005; *Bohling et al.*, 2007]. The overlying silt and clay provide an effective confining unit over the timescales involved in pumping tests described here, and we have modeled the drawdown responses assuming confined conditions. We have also assumed that the vertical hydraulic conductivity is equal to the horizontal conductivity at the scale of the depiction employed in this study (with the K field discretized into constant-K cells of dimension 1.5 m (5 feet) horizontal by 0.76 m (2.5 feet) vertical), since we have not seen evidence of significant anisotropy in these sediments.

[8] *Bohling et al.* [2007] provide details regarding the field implementation of the tomographic pumping tests investigated in this paper, so only a brief summary is provided here. Figure 1 shows the experimental configuration for the tests. The line segments on the left and right sides of the plot represent the sequence of pumping intervals in the two pumping wells, Gems4N and Gems4S. Both of these wells are constructed from 11-cm-diameter PVC pipe and are screened throughout the aquifer thickness. We performed 23 pumping tests, 12 with pumping in Gems4S and 11 with pumping in Gems4N. Each test involved pumping over a 0.6-m interval isolated by a pair of packers. Drawdowns were measured in two observation wells, HTMLS1 and HTMLS2, situated between Gems4N and Gems4S as shown in Figure 1. HTMLS1 and HTMLS2 are constructed from seven-chamber PVC pipe with a single screened opening in each chamber, each at a different sampling depth [*Einarson and Cherry*, 2002]. Only the six outer chambers of each sampler were employed in these tests (the seventh, central chamber was not used), resulting in six potential measurement locations at each sampler, or a total of 12 observation locations altogether. The circles in Figure 1 represent the sample port locations in HTMLS1 (1S through 6S, closer to Gems4S on the southern end of

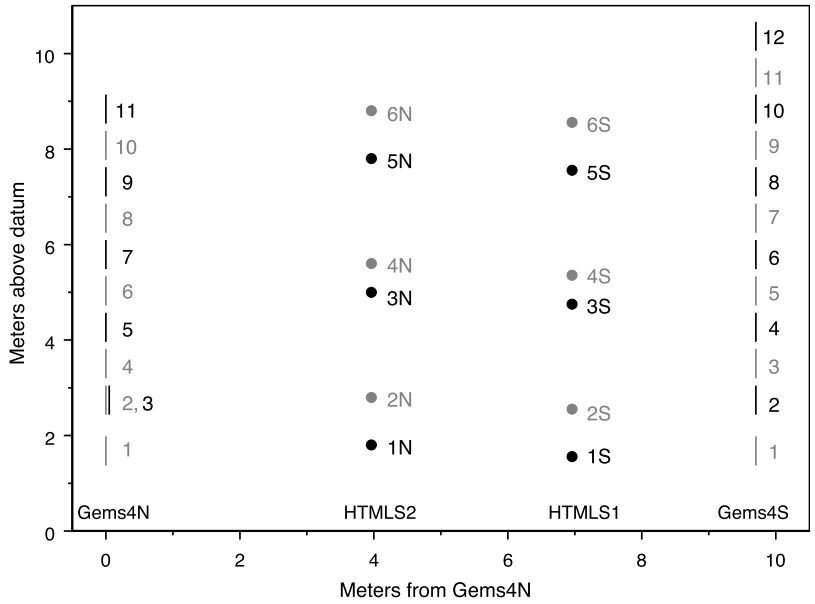

Figure 1. Tomographic pumping test sequence. Gems4N and Gems4S are pumping wells, and HTMLS1 and HTMLS2 are multichamber observation wells with six sample ports each. Black circles indicate sample ports used in tests with pumping intervals represented by black line segments, and similarly for gray circles and line segments.

the profile) and HTMLS2 (1N through 6N, closer to Gems4N on the northern end of the profile).

[9] During each test, we used six pressure transducers to monitor drawdowns at three of the six ports in each sampler. The pressure transducers were relocated between tests in a fashion that created a roughly uniform utilization of the 12 sample ports over the 23 tests. The odd-numbered ports were used for those tests whose pumping intervals are represented by black line segments in Figure 1, and the even-numbered ports for those represented with gray line segments. Essentially, a different set of ports (odd-numbered or even-numbered) was used for every other test in the vertical sequence. We did not monitor drawdown in the pumping intervals due to the difficulty of obtaining accurate drawdown measurements in a pumping well [*Driscoll*, 1986]. For each test, drawdown measurements were collected at a sample rate of 2 Hz (two samples per second) for at least 900 s (15 min) after the initiation of pumping. As discussed by *Bohling et al.* [2007], plots of drawdown responses indicate that steady-shape conditions seem to be attained within about 20 to 30 s after initiation of pumping within the region of investigation (ROI), which is in keeping with the expected time frame based on average aquifer properties.

[10] The analyses by *Bohling et al.* [2007] focused on the drawdown data obtained between 20 and 70 s after the initiation of pumping for each test. These data exhibit the constant, common slope versus log time and roughly constant differences in drawdown between different locations that are indicative of steady-shape flow [*Bohling et al.*, 2007, Figure 7]. *Bohling et al.* [2007] show that based on the average aquifer properties, steady-shape flow should be established around 20 to 30 s after initiation of pumping. Once steady-shape conditions are established, the storage properties of the ROI no longer influence the drawdown responses. In addition to the steady-shape character exhibited by the 20–70 s data, *Bohling et al.* [2007] chose to focus on this interval because drawdown responses during a number of tests exhibited changes in slope at later times, which we attribute to interference from pumping at high-capacity water supply wells in the vicinity of GEMS, and because early time data (prior to 20 s) exhibit oscillations due to inertial effects in the pumping well [*Butler and Zhan*, 2004]. Of course, the simulated values used in this sensitivity study are not affected by such factors, so we have more freedom in the selection of data intervals to consider. For the transient analyses, we have chosen to examine both an earlier time data record, from 0 to 30 s, and a longer-term record, from 0 to 300 s. The shorter time frame is chosen as one in which we might expect to see a nonnegligible influence of storage within the ROI on drawdown. For the sensitivity and resolution analyses based on a steady-shape formulation, this study focuses on drawdown responses from the 20–70 s interval, as in the work by *Bohling et al.* [2007].

3. Analysis Methodology

[11] This study uses a two-dimensional radial-vertical finite difference flow model implemented in Matlab, very similar to the Fortran program described by *Bohling and Butler* [2001]. Under conditions of radial symmetry, meaning the absence of angular variations in both the aquifer properties and the boundary conditions, the flow to a partially penetrating well pumping at a constant rate in a confined aquifer of infinite areal extent is described by

$$\frac{1}{r}\frac{\partial}{\partial r}\left(rK_r\frac{\partial s}{\partial r}\right)+\frac{\partial}{\partial z}\left(K_z\frac{\partial s}{\partial z}\right)=S_s\frac{\partial s}{\partial t}, \tag{1a}$$

where s = drawdown [L], S_s = specific storage [1/L], K_r, K_z = hydraulic conductivity in the radial and vertical directions,

t = time [T], r = radial coordinate [L], and z = vertical coordinate (positive upward from base of aquifer) [L], with upper and lower boundary conditions given by

$$\left[\frac{\partial s}{\partial z}\right]_{z=0} = 0 \tag{1b}$$

$$\left[\frac{\partial s}{\partial z}\right]_{z=B} = 0, \tag{1c}$$

where B is the thickness of the aquifer, an outer boundary condition given by

$$s(r=\infty, z, t) = 0 \tag{1d}$$

and an inner boundary condition given, in its simplest form, by

$$\left[K_r r \frac{\partial s}{\partial r}\right]_{r=r_w} = \begin{cases} \dfrac{Q}{2\pi b} & \text{if } z_b \le z \le z_t \\ 0 & \text{otherwise} \end{cases}, \tag{1e}$$

where r_w is the well radius, Q is the pumping rate, b is the thickness of the pumping interval, and z_b and z_t are the vertical coordinates of the bottom and the top of the pumping interval.

[12] In fact, the model uses a somewhat more complicated representation of the inner boundary condition than that shown in equation (1e), with a column of nodes of high and low K values representing the open portions of the well-bore and the packers, respectively [*Settari and Aziz*, 1974; *Rushton and Chan*, 1977; *Bohling and Butler*, 2001]. As explained by *Bohling et al.* [2007], the motivation for including the column of high K cells in the model is to account for the damping of vertical gradients due to bypass flow along the well-bore. In addition, the storage properties of the well-bore cells are set to represent well-bore storage effects, which influence the early time data in transient simulations. Similarly, *Vesselinov et al.* [2001a] explicitly incorporated open boreholes into their model of pneumatic tomography tests at the Apache Leap Research Site in order to account for the ability of the boreholes to store and transmit air. Thus the present study investigates the sensitivity and resolution accounting for the presence of the well-bore. Compared with simulating these tests without accounting for well-bore effects, bypass flow along the well-bore increases the sensitivity to aquifer K in the immediate vicinity of the well, because the vertical distribution of aquifer K adjacent to the well has a greater overall influence on the vertical distribution of flux than it would if the pumping intervals were perfectly isolated, and well-bore storage leads to a reduction in overall sensitivity to aquifer storage. Accordingly, well-bore effects lead to a relative increase in the resolution of aquifer K variations in the vicinity of the pumping wells and a general decrease in the resolution of variations in aquifer storage. Otherwise, the spatial distributions of parameter resolution in the absence of well-bore effects are similar to those shown in this paper.

[13] The model uses a logarithmic transform of the radial coordinate, $r' = \ln(r/r_w)$, to transform the radial flow problem into an equivalent Cartesian problem in (r',z) space [*Butler and McElwee*, 1995; *Bohling and Butler*, 2001]. We have used a simulation grid with 60 cells of dimension $\Delta r' = 0.2$ along the transformed radial axis and 70 cells of dimension $\Delta z = 0.152$ m (0.5 feet) along the vertical axis. In physical space, the radial location of the grid node with radial index i is $r_w \exp((i-0.5)\Delta r')$ and the location of the outer face of the corresponding cell is $r_w \exp(i\Delta r')$. This exponentially telescoping grid in the radial direction allows for a more detailed representation of aquifer property variations in the vicinity of the pumping well and a coarser representation with increasing distance from the pumping well, reflecting the fundamental sensitivity behavior of radial flow [*Butler*, 1990]. It also provides an easy means to place the outer boundary far from the pumping well. The discretization used here places the zero-drawdown outer boundary of the model about 9300 m from the pumping well, so that this boundary has negligible impact on transient drawdown simulations within the time frame of the pumping tests and on the simulated steady-shape drawdown configurations.

[14] To simulate tests with pumping in Gems4N, shown on the left (north) in Figure 1, we use a flow model whose radial axis originates at Gems4N and extends to the right, representing a vertical wedge encompassing the observation points and terminating in the outer boundary far to the right (south). Similarly, the tests with pumping in Gems4S use a model originating from Gems4S and extending to the left. Although we have used a cylindrical coordinate flow model to accurately represent the radial flow to each well, for the sake of the sensitivity and resolution analyses, we have parameterized the K and S_s variations on a common Cartesian grid representing the vertical plane encompassing Gems4N and Gems4S. The simulations described below use a parameter grid with 20 cells of dimension $\Delta x = 1.52$ m (5 feet) in the horizontal direction and 14 cells of dimension $\Delta z = 0.76$ m (2.5 feet) in the vertical direction. The parameter grid is centered on the midpoint between Gems4S and Gems4N, extending from 10.4 m to the left of Gems4N to 10.4 m to the right of Gems4S as viewed in Figure 1.

[15] For a given pumping test, the Cartesian (parameter) grid K and S_s values are mapped into the radial (simulation) grid originating from the pumping well for that test, as illustrated schematically in Figure 2. The parameter and simulation grids have been constructed so that each parameter grid cell incorporates exactly five simulation grid cells in the vertical direction, or conversely so that no simulation grid cell spans a vertical cell boundary in the parameter grid. This eliminates the need to account for property variations in the vertical direction within a single simulation grid cell. However, because of the telescoping nature of the simulation grid in the radial direction, it is inevitable that some simulation grid cells will span two or more parameter grid cells radially. In this case, the parameter values for the simulation grid cell are averages of the properties for the contributing parameter grid cells. Specifically, the K_r value for a given simulation grid cell is the harmonic average of the K_r values for the included parameter grid cells, weighted according the radial thickness of each parameter grid cell within the simulation grid cell, since the parameter-cell K_r values act in series to form the simulation-cell K_r value. The simulation-cell K_z value is a radial-thickness-weighted

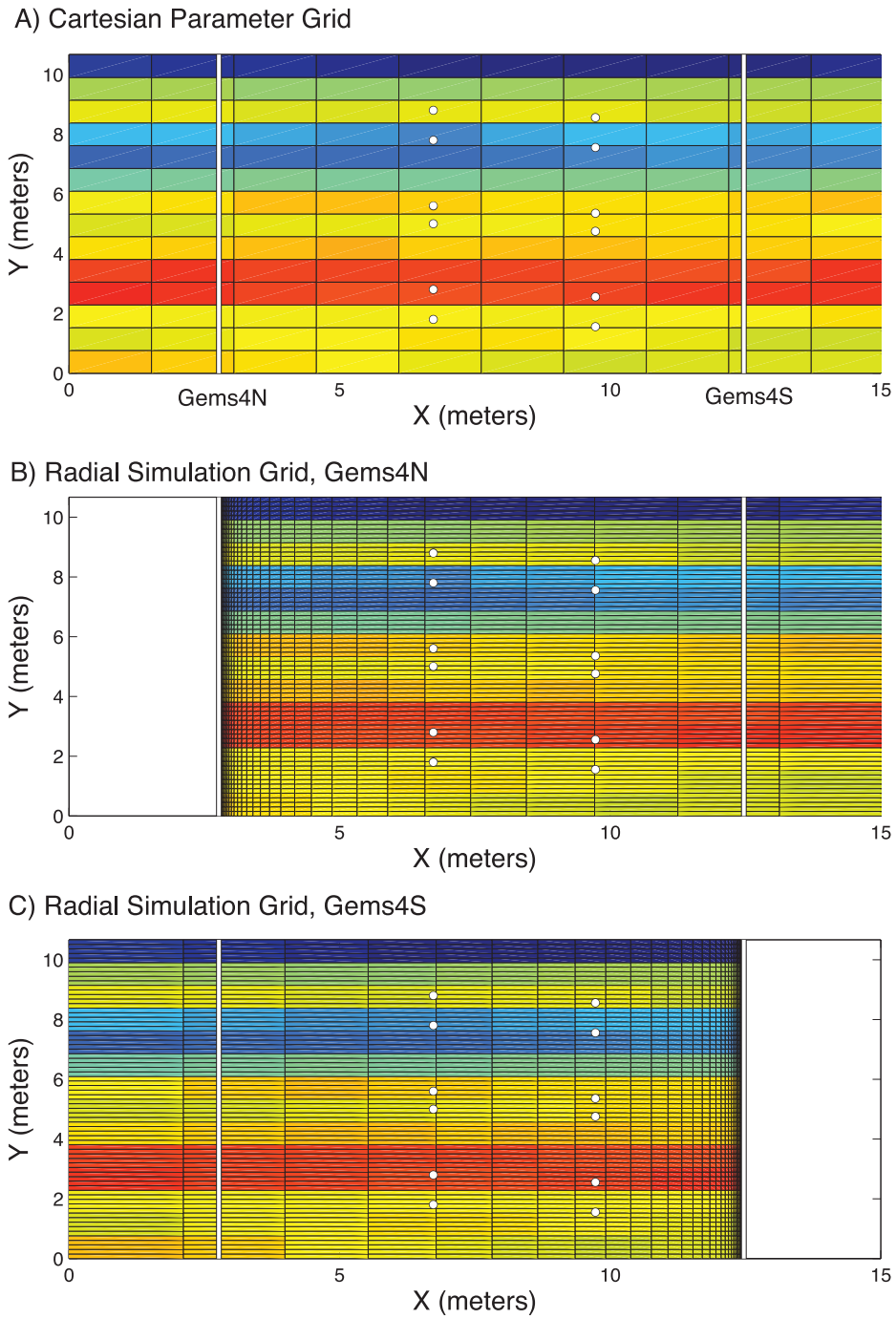

Figure 2. Schematic representation of mapping of a parameter (K or S_s) field from (a) the Cartesian parameter grid into (b) radial simulation grid for Gems4N and (c) the radial simulation grid for Gems4S. The color scale represents the variation of the parameter under consideration.

arithmetic average of the parameter-cell K_z values, since the contributing parameter cell K_z values act in parallel relative to flow in the vertical direction. The simulation-cell S_s values are also radial-thickness-weighted arithmetic averages, in this case representing a simple volumetric average of the contributing parameter-cell values. Simulation cells outside the extent of the parameter grid are populated with the bulk average property values of $K = 1.5 \times 10^{-3}$ m/s and $S_s = 1.2 \times 10^{-4}$ m^{-1}, the optimal effective homogeneous parameter values based on a transient analysis of the 20–70 s data from all 23 tests.

[16] Because the sensitivity and resolution analyses presented below use base values representing both homogeneous and isotropic conditions ($K_z = K_r$ for each parameter grid cell), the preceding discussion of averaging may seem immaterial to the present study. However, because we are considering sensitivity with respect to variations of the parameters on the Cartesian grid, these parameters are conceptually heterogeneous despite the use of homogeneous

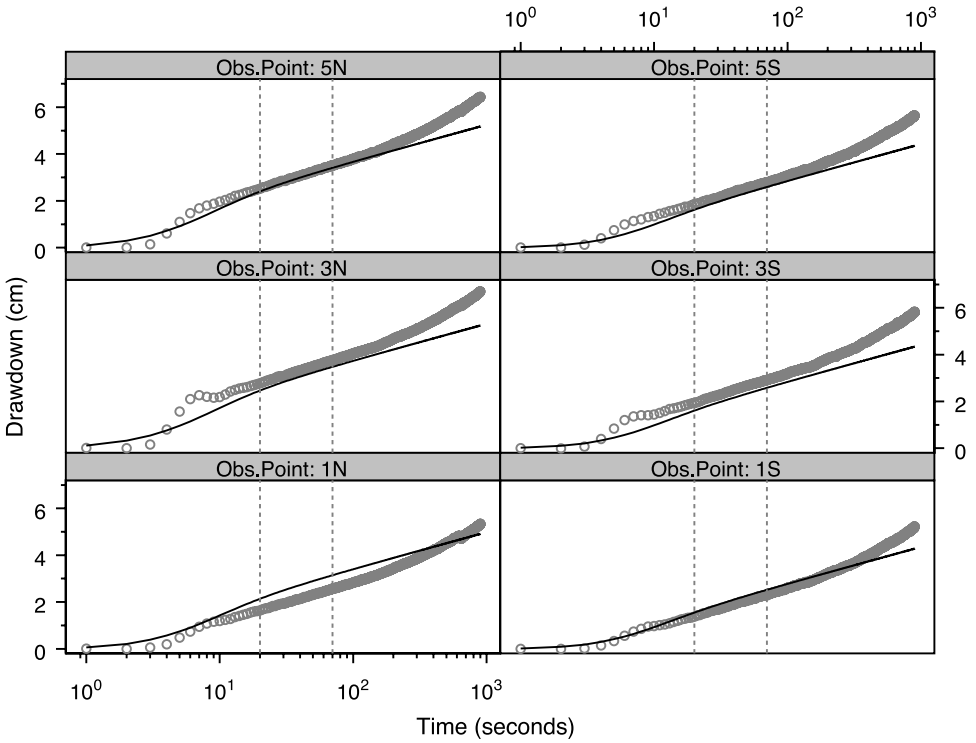

Figure 3. Drawdown data from test 7 in Gems4N (points) along with drawdowns predicted using best fit homogeneous parameters from analysis of 20–70 s data from all 23 tests (lines).

base values in the analyses. In fact, the sensitivities are computed using finite perturbations of the Cartesian grid cell values, resulting in perturbed parameter fields that are in fact heterogeneous, even if only slightly. It is important to point out that the process of mapping from the common Cartesian parameter grid into the appropriate radial grid for each test should not be confused with the subsequent step of transforming the radial flow problem into an equivalent Cartesian flow problem using the logarithmic transformation of the radial coordinate. The former is a mapping between two different grids in physical space, while the latter is a mathematical transformation that simplifies the solution of the radial flow problem.

[17] Finally, we must address the implications of using a radially symmetric flow model (assuming constant properties in the angular direction) while simultaneously entertaining the possibility of lateral property variations in the Cartesian parameter grid. Using a radially symmetric flow model means that each pumping test is treated as if the parameter fields, exhibiting both radial and vertical variations under general conditions, is the same in all azimuthal directions from the pumping well. This is clearly an unrealistic representation of true three-dimensional parameter variation, and, strictly speaking, the two radial grids produced by this mapping process would show inconsistent representations of the parameter variations outside the region between the two wells, if they were considered truly 3-D radial grids. However, an analysis using this representation will still provide a reasonable approximation of drawdown responses measured in the plane between the two pumping wells as long as the lateral heterogeneity is not extreme enough to induce significant angular variations in flux toward the well. In the absence of significant angular variations in flux, the flow along any particular angular wedge emanating from the well can be treated in isolation as a two-dimensional (radial-vertical) problem bounded by zero-flux boundaries in the angular direction. Such variations are not a concern for the first-order sensitivity analysis presented here, since it is based on small perturbations from a homogeneous, and therefore radially symmetric, base case. However, one would have to consider the implications of the assumption of radial symmetry more carefully in an inverse analysis involving significant lateral property variations and potentially significant angular variations in flux.

[18] In summary, we have used a two-dimensional radial-vertical flow model in order to accurately represent the physics of the flow problem while focusing the sensitivity analysis on the properties of the plane containing the pumping and observation wells. We have used a common, Cartesian parameter grid along this plane as a convenient framework for parameterizing the sensitivity analysis, mapping the Cartesian grid properties into the appropriate radial grid for each test. It should be kept in mind that a two-dimensional Cartesian (x–z) flow model would not provide a physically correct representation of the radial flow geometry, since it would artificially restrict the flow to this vertical plane.

4. Temporal Sensitivity Behavior for a Single Test

[19] Before embarking on a complete sensitivity analysis of tomographic pumping test responses to spatial variations in K and S_s, it is instructive to examine some fundamental aspects of the sensitivity behavior for a single pumping test. In this section we will focus on the drawdown responses for test 7 in Gems4N, as illustrated in Figures 3 and 4. Figure 3

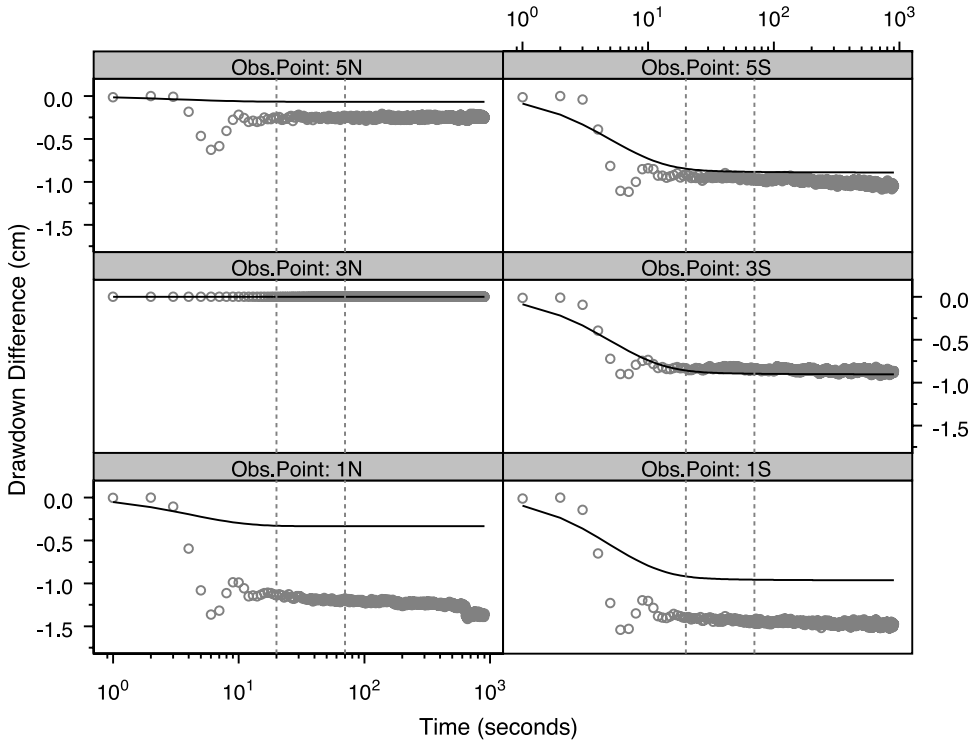

Figure 4. Drawdown differences relative to drawdown at observation point 3N during test 7 in Gems4N (points), along with differences predicted using best fit homogeneous parameters from analysis of 20–70 s data from all 23 tests (lines).

shows the full 900 s of drawdown data obtained at the six observation points for this test, along with curves representing the drawdowns simulated using the optimal effective uniform parameter values, $K = 1.5 \times 10^{-3}$ m/s and $S_s = 1.2 \times 10^{-4}$ m^{-1}, obtained from fitting the drawdown data between 20 and 70 s for all 23 of the tomographic pumping tests. In this analysis we will compute sensitivities based on these optimal effective uniform values of K and S_s, but formally divided for the sake of sensitivity analysis into a region within 10.4 m of Gems4N and a region beyond 10.4 m from Gems4N. The distance 10.4 m is chosen as the nearest cell boundary distance to 10 m, given the radial discretization of the finite difference model. This division separates the aquifer into two zones, one roughly representing the region of investigation (ROI) encompassed by the test wells and the other representing the aquifer outside the ROI. This exercise provides basic physical insight into how the bulk K and S_s values within and outside the ROI influence the drawdown responses in the ROI. For the sake of demonstrating aspects of the sensitivity behavior relating to the steady-shape inversion approach, this section will also examine the sensitivities of drawdown differences to the aquifer properties. Figure 4 shows the same data as Figure 3, but now in terms of differences in drawdown relative to that at sample port 3N, both for the observed drawdowns from this test and those simulated using the optimal effective uniform parameter values. Since these uniform parameter values represent a compromise fit to the 20–70 s data from all 23 tests, they do not produce a particularly good fit to the full data record from this specific test. The point, however, is that the simulated curves show the same general behavior as the observed drawdowns, indicating that these parameter values are reasonable for this sensitivity study.

[20] Figure 5 shows the sensitivities of the drawdowns to the K and S_s values within and beyond 10.4 m from Gems4N over the entire 900 s of data. The plotted sensitivities are normalized by the corresponding parameter values, that is,

$$K\frac{ds}{dK} = \frac{ds}{dK/K} = \frac{ds}{d(\ln K)} \tag{2a}$$

$$S_s\frac{ds}{dS_s} = \frac{ds}{dS_s/S} = \frac{ds}{d(\ln S_s)}. \tag{2b}$$

This normalization puts the sensitivities to the different parameters on an equal footing in terms of change of drawdown (in centimeters) in response to a unit relative change in the parameter value or unit change in the log of the parameter value.

[21] Several conclusions can be drawn from Figure 5. The first is that the sensitivity of drawdown to storage in the ROI, S_{s1}, is relatively small and also of finite duration, peaking at around 9 s and dying back to essentially zero by about 100 s. This means that high-quality early time data are required to accurately estimate the storage properties of this region. As mentioned above, much of the early time data observed in the GEMS tomographic pumping tests is influenced by inertial oscillations, largely obscuring whatever information S_{s1} might be contained in the drawdown responses. Although inertial oscillations are a particular problem associated with well tests in high-K aquifers [*Butler and Zhan*, 2004], early time data can also be

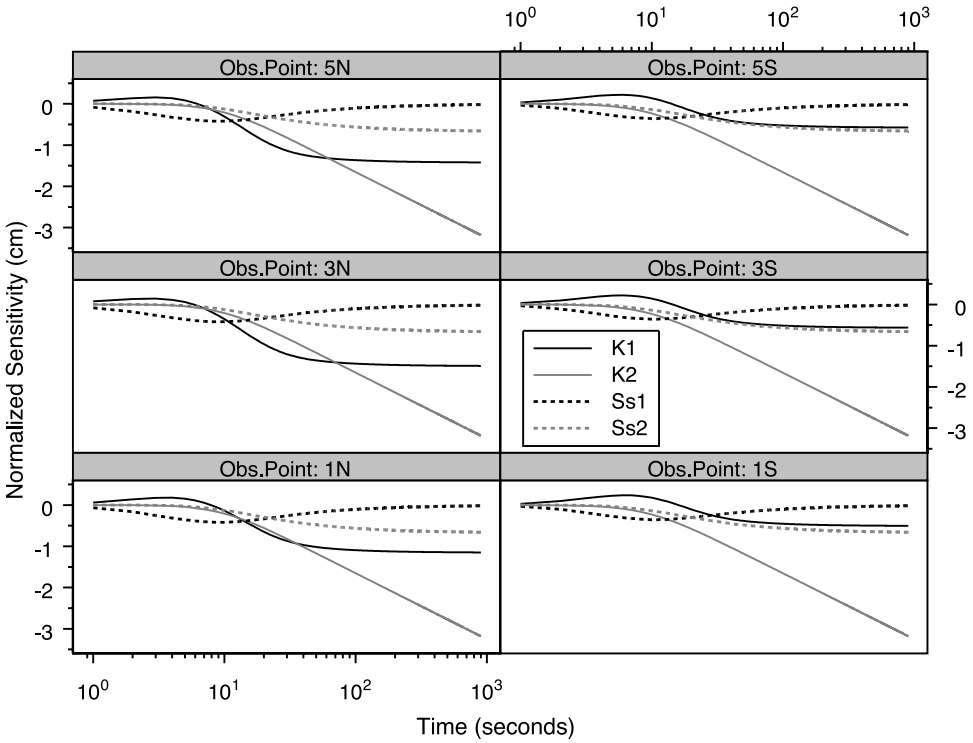

Figure 5. Sensitivities of drawdown at each observation point to properties within 10.4 m from pumping well (K_1, S_{s1}) and properties beyond 10.4 m from the pumping well (K_2, S_{s2}), based on best fit homogeneous model.

affected by other factors such as well-bore storage. Combined with the low magnitude of sensitivity to storage, these factors make it extremely difficult to obtain accurate S_s estimates in many settings. At later times, the sensitivities to S_{s2}, the specific storage outside the ROI, and the sensitivity to K_1, the hydraulic conductivity within the ROI, both level out to constant, nonzero values, while the sensitivity to K_2, the hydraulic conductivity outside the ROI, continues to increase. This means that at later times the changes in drawdown are controlled strictly by the K outside the ROI. The fact that the sensitivities to K_1 and S_{s2} level off to constant, nonzero values means that these two parameters act together to contribute a constant offset to the late-time drawdown data. As discussed by *Butler* [1990], these conditions explain the robustness of the Cooper-Jacob method [*Cooper and Jacob*, 1946] for the estimation of bulk hydraulic conductivity: At later times the slope on a drawdown versus log time curve is dictated by the bulk average K of the aquifer radially outward from the ROI. The fact that K_1 and S_{s2} both contribute to the constant offset means that the storage coefficient estimate obtained from a Cooper-Jacob analysis is in fact confounded by any unquantified K variations within the ROI. Furthermore, the fairly strong correlation of the sensitivities to these two parameters, as expressed by the similar shapes of the corresponding sensitivity curves in Figure 5, indicates that K_1 and S_{s2} will be difficult to estimate independently regardless of analysis method.

[22] These results corroborate the findings by *Butler* [1988], *Butler and McElwee* [1990], *Meier et al.* [1998], and *Sánchez-Vila et al.* [1999]: Analysis of drawdowns from constant-rate pumping tests generally yields reliable estimates of large-scale average K, but estimates of S_s are confounded by low sensitivity and correlation with K variations between the observation well and the pumping well.

[23] To provide some sense of the sensitivity behavior associated with the steady-shape analysis approach, which is based on the fitting of differences in drawdown between different locations, rather than drawdowns themselves, Figure 6 shows the sensitivities of drawdown differences relative to drawdowns at observation point 3N for test 7 in Gems4N. That is, these are the sensitivities of the drawdown differences illustrated in Figure 4 to the four properties, K_1, K_2, S_{s1}, and S_{s2}. It should be noted that the choice of 3N as the reference point is arbitrary and this plot is simply intended to illustrate a principle. The steady-shape analysis discussed by *Bohling et al.* [2007] used drawdown differences between all possible pairs of observation points at each observation time. Because Figure 6 shows sensitivities of differences relative to 3N, the sensitivities at 3N are exactly zero by construction and the sensitivities at the south observation ports (1S, 3S, and 5S) are larger due to their greater separation from 3N than the other two north observation ports. A different choice of reference point would result in a different spatial pattern of the magnitudes of the sensitivities, but the fundamental result would be the same: K_1 rapidly becomes the dominant control on differences between drawdowns in the ROI. After approximately 30 s the sensitivity to K_1 is very close to its final constant value, and the sensitivities to the other parameters are very close to their final values of zero. In fact, this corresponds to the onset of steady-shape flow conditions, in which the gradients have essentially reached their final steady state

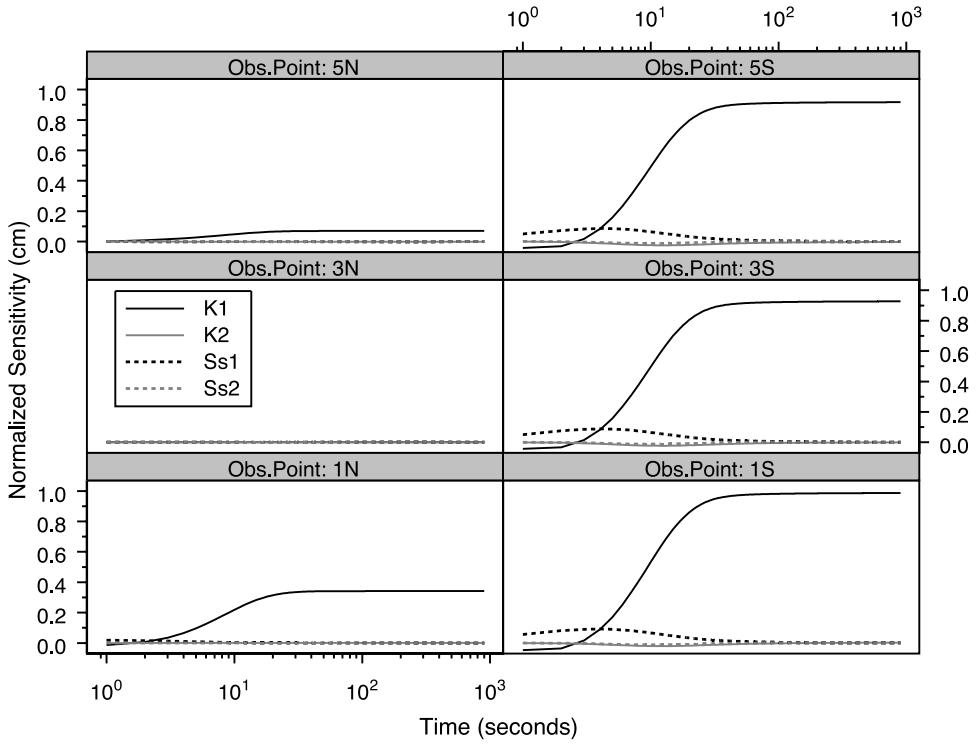

Figure 6. Sensitivities of drawdown differences relative to observation point 3N to properties within 10.4 m from pumping well (K_1, S_{s1}) and properties beyond 10.4 m from the pumping well (K_2, S_{s2})

values, although the drawdowns themselves are continuing to increase in a spatially uniform fashion throughout the ROI. These gradients are controlled by variations in K in the ROI, superimposed on the primary control of the boundary condition configuration, particularly the location of the pumping interval. Once steady-shape conditions are established, the uniform increase of drawdown versus time throughout the ROI is dictated by K_2, as noted in the discussion of Figure 5.

[24] Thus the steady-shape analysis approach, based on analysis of drawdown differences in the ROI, focuses on K variations in the ROI, effectively filtering out the influence of K variations outside the ROI and the influence of S_s everywhere. As the following discussion will illustrate, K variations outside the ROI and S_s variations throughout the problem domain are very difficult to resolve, even using a temporal analysis.

5. Sensitivity and Resolution: Transient Analysis

[25] In this section we will explore the sensitivity and resolution associated with a transient analysis of the drawdown records over two different time frames for all 23 pumping tests. This analysis is based on a Jacobian matrix computed from a simulation of the drawdown records for each test, again using the optimal effective uniform values for K and S_s as the base parameter values, as described above. Each entry in the Jacobian matrix represents the sensitivity of the drawdown at a given time and location, s_i, to one of the model parameters, p_j:

$$J_{i,j} = \frac{\partial s_i}{\partial p_j}. \tag{3}$$

The drawdown index i runs over all observation times and locations for all 23 tests, and p_j represents either the ln$K$ or lnS_s value associated with each of the cells in the Cartesian parameter grid. That is, the Jacobian used here is built from the normalized sensitivities, or sensitivities to logarithmic parameter values, defined in equation (2), so that the resolution results presented represent the ability to resolve relative variations in the K and S_s values using a given test configuration. The Jacobian matrix represents a linear approximation of the behavior of the flow model in the vicinity of the parameters used in the simulation [*Sun*, 1994; *Vasco et al.*, 1997]. In inverse modeling, it is fairly common to compute linear confidence intervals for the estimated parameters based on the Jacobian matrix evaluated for those parameters. *Vasco et al.* [1997] point out that the Jacobian can also be used in the assessment of model resolution, using techniques developed for linear models in the context of geophysical data inversion [e.g., *Menke*, 1989; *Aster et al.*, 2005]. *Vasco et al.* [1997] present resolution results associated with a regularized inversion, investigating the tradeoff between parameter resolution and parameter variance when a regularization term is introduced to constrain estimated parameters to reasonable values. In this case, increasing the degree of regularization necessarily reduces the resulting parameter resolution, a manifestation of the classic bias-variance tradeoff of statistical model fitting [*Hastie et al.*, 2001].

[26] In this study we investigate the resolution associated with the tomographic pumping tests in the absence of an explicit regularization term using a truncated singular value decomposition (TSVD) of the Jacobian matrix, as described

by *Aster et al.* [2005]. The singular value decomposition of the Jacobian matrix, **J**, is given by

$$\mathbf{J} = \mathbf{USV}, \tag{4}$$

where **S** is a diagonal matrix with a set of nonnegative diagonal elements referred to as the singular values of **J**, and **U** and **V** are unit orthogonal matrices holding the left and right singular vectors of **J**. The singular values are arranged in order of decreasing magnitude along the diagonal of **S**, with the columns of **U** and **V** arranged in a corresponding order. The columns of **V** represent linear combinations of the model parameters (unknown $\ln K$ and $\ln S_s$ values), and the leading columns, corresponding with the largest singular values, represent the linear combinations that are most strongly resolved by the data. *Tonkin and Doherty* [2005] refer to these linear combinations of parameters as "superparameters" in their discussion of the application of truncated SVD inversion to groundwater problems. Columns of V associated with smaller singular values represent more poorly resolved combinations of parameters. A truncated singular value inversion retains only the p largest singular values and vectors in constructing the Moore-Penrose pseudoinverse [*Aster et al.*, 2005] of the matrix in question, in this case the Jacobian matrix:

$$\mathbf{J}_p^{\dagger} = \mathbf{V}_p \mathbf{S}_p^{-1} \mathbf{U}_p^T. \tag{5}$$

The Moore-Penrose pseudoinverse can be applied to an arbitrary rectangular matrix. This pseudoinverse can be used in computing an $n \times 1$ vector of estimated parameters, **m**, from an $m \times 1$ vector of observed data, **d**, as

$$\mathbf{m} = \mathbf{J}_p^{\dagger} \mathbf{d}. \tag{6}$$

In the case of a Jacobian matrix for an inverse problem with the number of (independent) data m exceeding the number of unknown parameters n, the rank of **J** will be limited by the number of parameters, meaning there will be at most n nonzero singular values. Using $p = n$ in the computation of the pseudoinverse will yield an estimated parameter vector **m** that is as close as possible to the "exact" solution for this problem (a least squares solution since $m > n$). Retaining a large number of singular values and vectors in the pseudoinverse will allow a better fit to the observed data and a better apparent resolution of the detail in the estimated parameters, but the price paid for this improvement is that the terms associated with smaller singular values will tend to amplify noise in the observed data, leading to a higher variance in the parameter estimates.

[27] Retaining a smaller set of terms associated with larger singular values will result in estimates with lower variance, representing linear combinations of the better resolved "superparameters" in the parlance of *Tonkin and Doherty* [2005]. The price paid for these lower-variance estimates is some bias in the estimated parameters. This bias can be characterized in terms of the smoothing, relative to a "true" model, introduced by the truncation. Following the development of *Aster et al.* [2005], if the true model is represented by **m** and the corresponding true data vector is represented by $\mathbf{d} = \mathbf{Jm}$, then the parameter vector estimated from application of the pseudoinverse would be

$$\mathbf{m}_{\dagger} = \mathbf{J}_p^{\dagger} \mathbf{Jm}. \tag{7}$$

The matrix multiplying the true model is the model resolution matrix

$$\mathbf{R} = \mathbf{J}_p^{\dagger} \mathbf{J} = \mathbf{V}_p \mathbf{V}_p', \tag{8}$$

which represents the degree of smoothing or blurring inherent in the truncated SVD inversion. As described by *Vasco et al.* [1997], the ith row of **R** is a set of averaging weights, with entry $\mathbf{R}_{i,j}$ representing the influence of the jth model parameter on the estimate of the ith parameter. Perfect model resolution would be represented by $\mathbf{R} = \mathbf{I}$, the identity matrix, meaning that each parameter is perfectly resolved ($R_{i,i} = 1$) without any confounding influence from other parameters ($R_{i,j} = 0$ for $j \neq i$).

[28] It should be remembered that most groundwater inverse problems are inherently nonlinear, and are typically solved in a number of steps, with the Jacobian matrix serving as an approximate linear representation of the nonlinear flow or transport model at each step. In this case, the vector **d** represents the matrix of residuals between the observed data values and corresponding simulated values at the current step and **m** represents a vector of parameter updates. Following the approach of *Clemo et al.* [2003], this study will assume that **J** represents a Jacobian computed based on a true or final parameter vector, so that **d** represents a final residual vector and **m** represents a proposed final update, providing a basis for computations of fit diagnostics. In this case, the Jacobian is computed using the optimal homogeneous parameters discussed above. In fact, **d** will be taken as a "pure noise" residual vector following a Gaussian distribution with a standard deviation of 2×10^{-4} m, which seems to be a reasonable order of magnitude estimate for the error in the drawdown measurements during the tomographic pumping tests at GEMS [*Bohling et al.*, 2007]. As described earlier, the sensitivities in the Jacobian matrix are normalized (or, alternatively, are sensitivities to the log parameter values), so that **m** can be taken as vector of relative parameter updates. With **d** taken to represent pure noise, **m** can be interpreted as the error or variation in the parameters resulting from the noise in the data. That is, the norm of **m** in this case is a measure of the noise amplification error [*Vogel*, 2002]. As more terms are added to the truncated SVD, the magnitude of **m** increases, reflecting the increasing amplification of noise associated with the increasing demand for resolution. For consistency among the different cases presented here, the resolution matrices will be computed based on threshold noise levels in **m**, retaining however many terms are required to produce root-mean squared values of 0.01 and 0.1 for the entries in **m**, i.e., the number of terms that amplify the assumed drawdown data standard deviation of 2×10^{-4} m into average relative errors of 1% and 10% in the parameter estimates.

[29] The analysis is applied over two different sample time frames, one extending from 1 to 300 s after the initiation of each test and the other extending from 1 to 30 s after the initiation of each test, using a 1-s sample

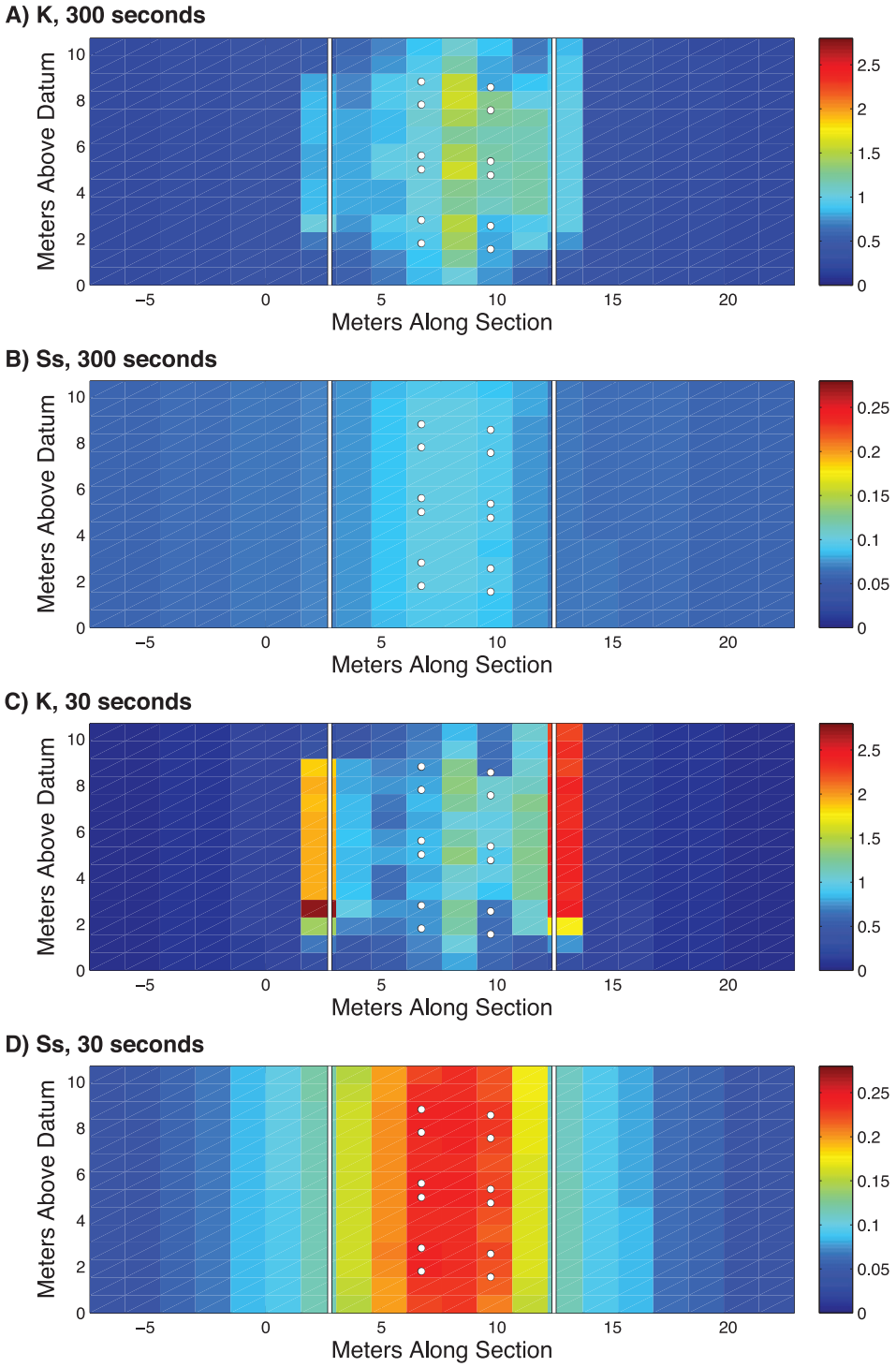

Figure 7. Root-mean-square normalized sensitivity to K and S_s over all 23 tests for transient analysis of drawdown records of different lengths: (a) K, 300 s, (b) S_s, 300 s, (c) K, 30 s, and (d) S_s, 30 s. Note differences in scale for sensitivity to K (Figures 7a and 7c) and sensitivity to S_s (Figures 7b and 7d).

spacing in both cases. As can be seen from Figure 5, the 300-s time frame approximately covers the full development of the sensitivity curves discussed in the previous section; after 300 s these curves have reached their final values (constant values for both storage values and K within the ROI, constant slope for K outside the ROI). Because the sensitivities to the K values quickly become dominant, examining the sensitivity and resolution results over this longer time frame could be considered to bias the analysis in favor of K. Therefore we also present a sensitivity and resolution analysis based on the first 30 s of data for each test, the period during which we might expect to see some significant sensitivity to the specific storage within the ROI.

[30] Figure 7 shows the root-mean-square (RMS) normalized sensitivity of drawdown observations over all 23 tests to the K and S_s value for each cell in the 20 $\times$ 14 parameter

grid for both the 300-s and 30-s time frames. For increased generality, the results shown include a scaling by the assumed standard deviation of the drawdown measurements, σ_s, so that the RMS normalized sensitivity to the K value for cell j is given by

$$\sqrt{\frac{1}{n}\sum_{i=1}^{n}\left(\frac{1}{\sigma_s}K_j\frac{ds_i}{dK_j}\right)^2}=\sqrt{\frac{1}{n}\sum_{i=1}^{n}\left(\frac{1}{\sigma_s}\frac{ds_i}{d\ln K_j}\right)^2} \quad (9)$$

and similarly for S_s. The summation is over the entire set of n simulated drawdowns at all observation points and times over all tests. The total number of data for the analysis based on the 300-s time frame is 41,400 (300 observations at six observation points over 23 tests) and 4140 for the analysis based on the first 30 s of data. The RMS normalized sensitivity is an integrated measure of the sensitivity of the simulated drawdowns at all observation points and times to a small relative change in the K or S_s in a given cell. The (root) mean square, rather than sum square, sensitivities are displayed in Figure 7 in order to emphasize the relative variation of the sensitivities associated with each data record, factoring out the overall increase in sensitivity yielded by the longer record. It is these relative variations within each record, rather than the overall magnitude of the Jacobian matrix, that determine the parameter correlation structure reflected in the resolution matrix.

[31] For the interpretation of Figure 7, it is first important to note the difference in scale between the plots of sensitivity to K and sensitivity to S_s: The peak sensitivities to relative variations in K (or equivalently, to ln$K$) are roughly an order of magnitude larger than the peak sensitivities to relative variations in S_s (or to lnS_s). This is another indication of the dominating influence of K on drawdown responses. The RMS normalized sensitivities based on the 30-s records indicate that the early time data do indeed show a larger relative sensitivity to S_s than the 300-s data records, as expected, although that sensitivity is still small in comparison with the sensitivity to K.

[32] In all cases, it is clear that the sensitivity to the K or S_s of a fixed volume (in this case, a parameter grid cell) is much higher if that volume is within the region of investigation for these tests and drops off rapidly outside that region. This may seem contradictory to the earlier discussion of the time variation of sensitivities in a single test, demonstrating an increasing sensitivity over time to K outside the ROI (Figure 5). However, that result is for the bulk K of the entire region outside the ROI, rather than sensitivities to K values of a specified volume of material at different locations. The sensitivity patterns shown in Figure 7 indicate that it will be almost impossible to extract information about variations in K or S_s outside the tested region, despite the fact that the bulk properties of this region have a significant influence on the drawdowns (Figure 5). Next, we will examine this behavior more quantitatively using resolution analysis.

[33] The RMS sensitivity values shown in Figure 7 are summaries of the full Jacobian matrices associated with the analyses of the 300-s or 30-s records. For the analysis of the 300-s records, the Jacobian matrix has n = 41,400 rows and m = 560 columns, the first 280 representing the K values over the parameter grid and the next 280 representing the S_s values. Similarly, the Jacobian for the analysis of 30-s records is 4140 × 560. In either case, the rank of the Jacobian is limited to 560, the number of parameters. Figure 8a shows the singular value spectra for both cases. A singular value spectrum is simply a plot of the singular values in descending order. The singular values have been scaled to the first (maximum) singular value in each case, so that both spectra start from 1. A steeper slope on the spectrum indicates a more rapid decrease in the ability to accurately estimate the parameter combinations (singular vectors) associated with successive singular values.

[34] In order to compare the resolution behavior for the two cases, we need some quantitative measure that we can use to truncate the two singular value spectra in a consistent fashion. We can find this in the degree of noise amplification associated with each problem. Figure 8b is a plot of the RMS model norm obtained when a truncated SVD inversion of the Jacobian in each case is applied to a pure noise data residual vector versus the number of terms (p in equations (5)–(8)) retained in the inversion. As mentioned above, the data residual vector is Gaussian with a mean of zero and a standard deviation of 2×10^{-4} m. The RMS model norm is a measure of the noise amplification error as described by *Vogel* [2002], based on a particular realization of the residual vector and treating the Jacobian as a linear approximation of the flow model in the vicinity of the base parameter values. Repeating the analysis with different realizations of the residual vector showed essentially the same model norm results.

[35] Figure 8b shows the noise amplification behavior for the two analysis scenarios, showing the price we pay in terms of increasing parameter variance as we add terms in a quest for increased resolution. For the analysis of 30-s records, retaining 55 terms in the inversion results in an RMS model norm or relative parameter error of 0.01, while retaining 104 terms leads to a relative parameter error of 0.1. For the analysis of 300-s records, these thresholds are reached at 84 terms and 119 terms. We now use these thresholds to compute the corresponding resolution matrices. That is, the resolution matrix associated with a relative parameter error of 1% for the analysis of 30-s records is computed using the first 55 right singular vectors of the Jacobian matrix for that case, while the resolution matrix associated with the 1% error level for the 300-s case is computed using the first 84 right singular vectors for that case.

[36] In each case, the resolution matrix is 560 × 560, with an upper left 280 × 280 matrix associated with the K values of the 280 parameter grid cells, a lower right 280 × 280 matrix associated with the S_s values of those cells, and lower left and upper right 280 × 280 matrices describing interactions among the K and S_s values. Each diagonal element describes the degree of resolution of the K or S_s value in a particular model cell and ranges from 1 for a perfectly resolved parameter to 0 for a completely unresolved parameter. Thus one simple means for examining the resolution behavior associated with a truncated SVD inversion is to plot the diagonal elements of the resolution matrix at the corresponding model cell locations [*Aster et al.*, 2005]. Off-diagonal elements of the resolution matrix describe the extent of blurring of a particular parameter estimate due to correlations with other parameters during the inversion process. Thus, as the diagonal element $R_{i,i}$

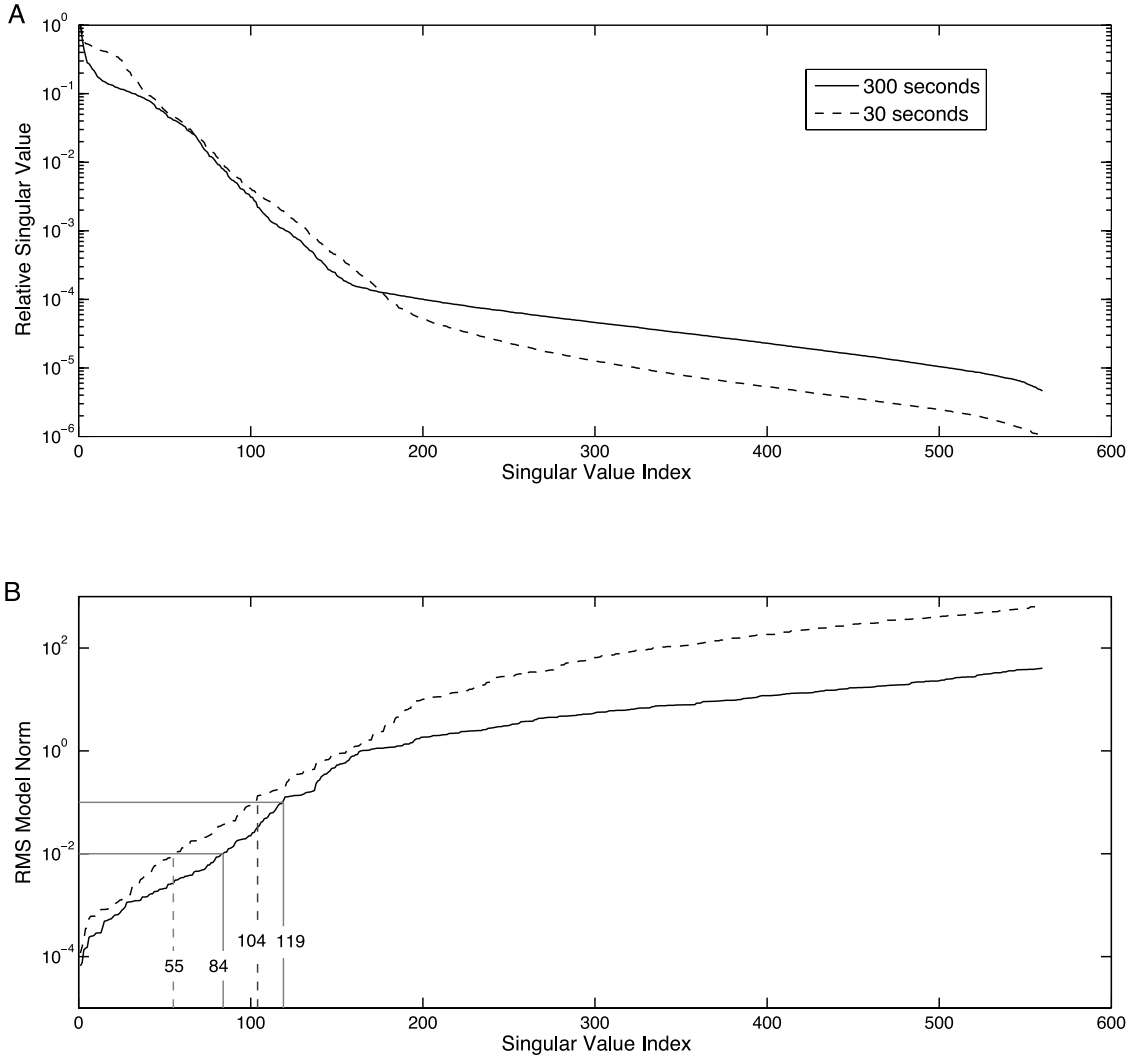

Figure 8. (a) Singular value spectra, and (b) root-mean-square model norm associated with truncated singular value decomposition (SVD) inversion of pure noise data vector for analysis of 300-s (solid line) and 30-s (dashed line) drawdown records.

decreases in magnitude, the would-be resolution for the corresponding parameter is spread to other elements, $R_{i,j}$, in the same row of the resolution matrix, so that an overall measure of the blurring associated with the inversion process is given by the norm of the deviation between R and the identity matrix, and a related spread measure associated with each parameter estimate can also be computed [*Clemo et al.*, 2003; *Menke*, 1989]. Here we will simply display the diagonal elements of **R**, the first 280 associated with the model cell K values and the second 280 associated with the model cell S_s values. Diagonal elements less than 0.5 indicate that the parameter estimate for a cell is influenced more strongly by other parameter values than it is by the corresponding property (K or S_s) of the cell itself.

[37] Figure 9 shows the resolution results associated with the analysis of the 300-s records from the 23 pumping tests based on truncated SVD inversion of the Jacobian matrix employing 84 singular values and 119 singular values. These clearly demonstrate the increase in resolution associated with retaining more terms in the inversion. However, it must be kept in mind that the cost of this improvement is an amplification of data noise. The 84- and 119-term inversions are associated with relative parameter error levels of 1% and 10% in the pure-noise inversion. It is also clear that the analysis of the 300-s drawdown records provides reasonable resolution only for K values within the ROI for the tests. K values outside the ROI and S_s values everywhere are very poorly resolved.

[38] Figure 10 shows the comparable resolution results for the analysis of the 30-s records from all 23 tests, for which the 55-term inversion is associated with a relative parameter error of 1% and the 104-term inversion is associated with a relative parameter error of 10%. Although focusing on the earlier-time data did produce an increase in the RMS normalized sensitivity to storage (Figure 7), comparing Figures 9 and 10 shows that this change in focus does not produce a significant increase in our ability to resolve variations in storage. It does, however, lead to a somewhat reduced resolution of the K variation. Any additional factors affecting early time data, such as wellbore storage or oscillatory behavior, would further obscure

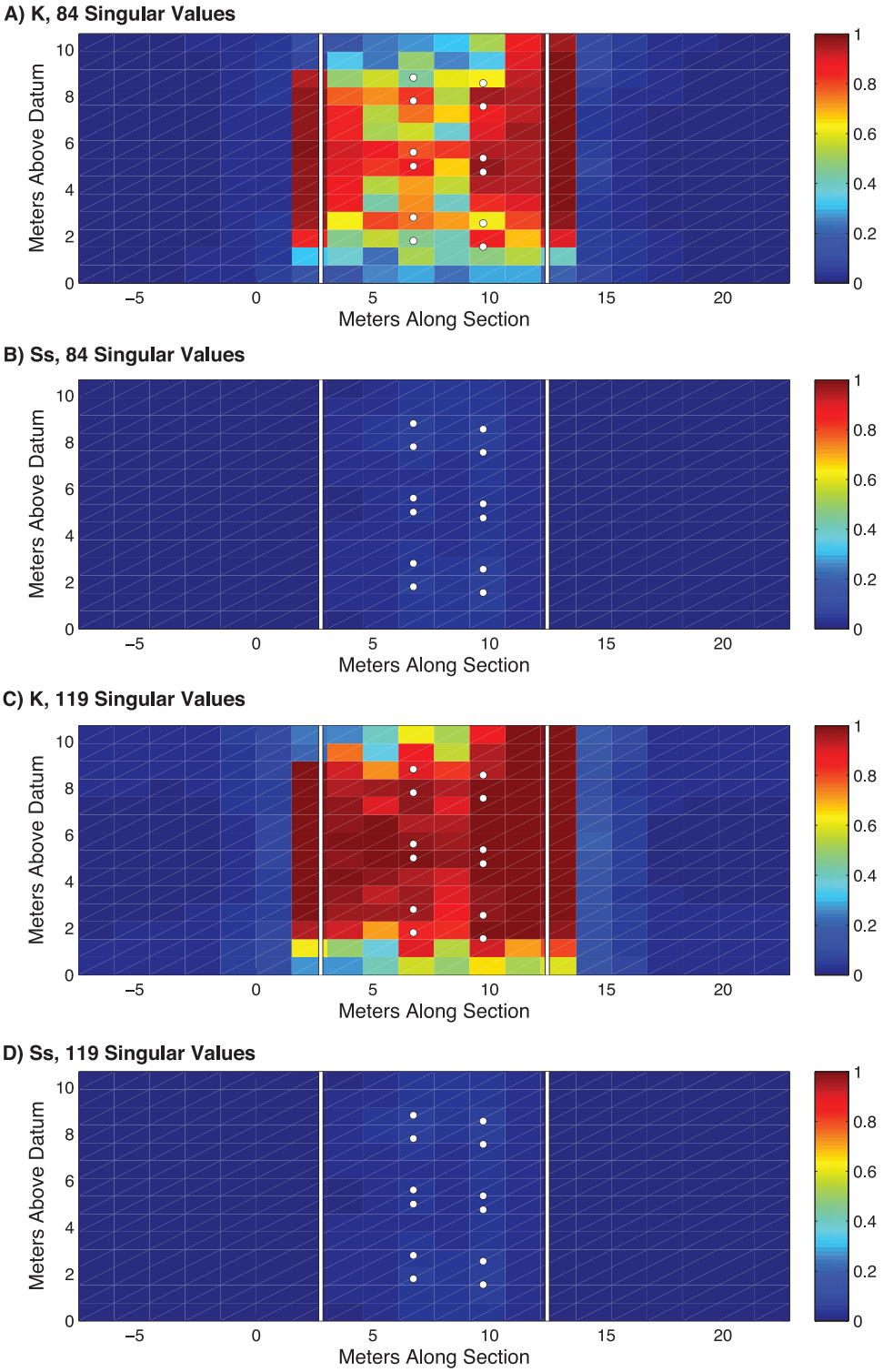

Figure 9. Diagonal elements of resolution matrix for analysis of 300-s drawdown records using truncated SVD inversion using 84 and 119 singular values: (a) K, 84 singular values, (b) S_s, 84 singular values, (c) K, 119 singular values, and (d) S_s, 119 singular values.

the information regarding storage variations that we might hope to extract from these data.

[39] *Zhu and Yeh* [2005] have pointed out that successive measurements in a drawdown record are highly correlated and recommend using a small selected subset of observations from early and late times to avoid a high degree of data redundancy. In that regard, the temporally dense data records used in this study exhibit a very high degree of correlation or redundancy. However, we are here using the truncated SVD precisely for the purpose of determining what independent information can be extracted from the drawdown data. As discussed by *Aster et al.* [2005], the

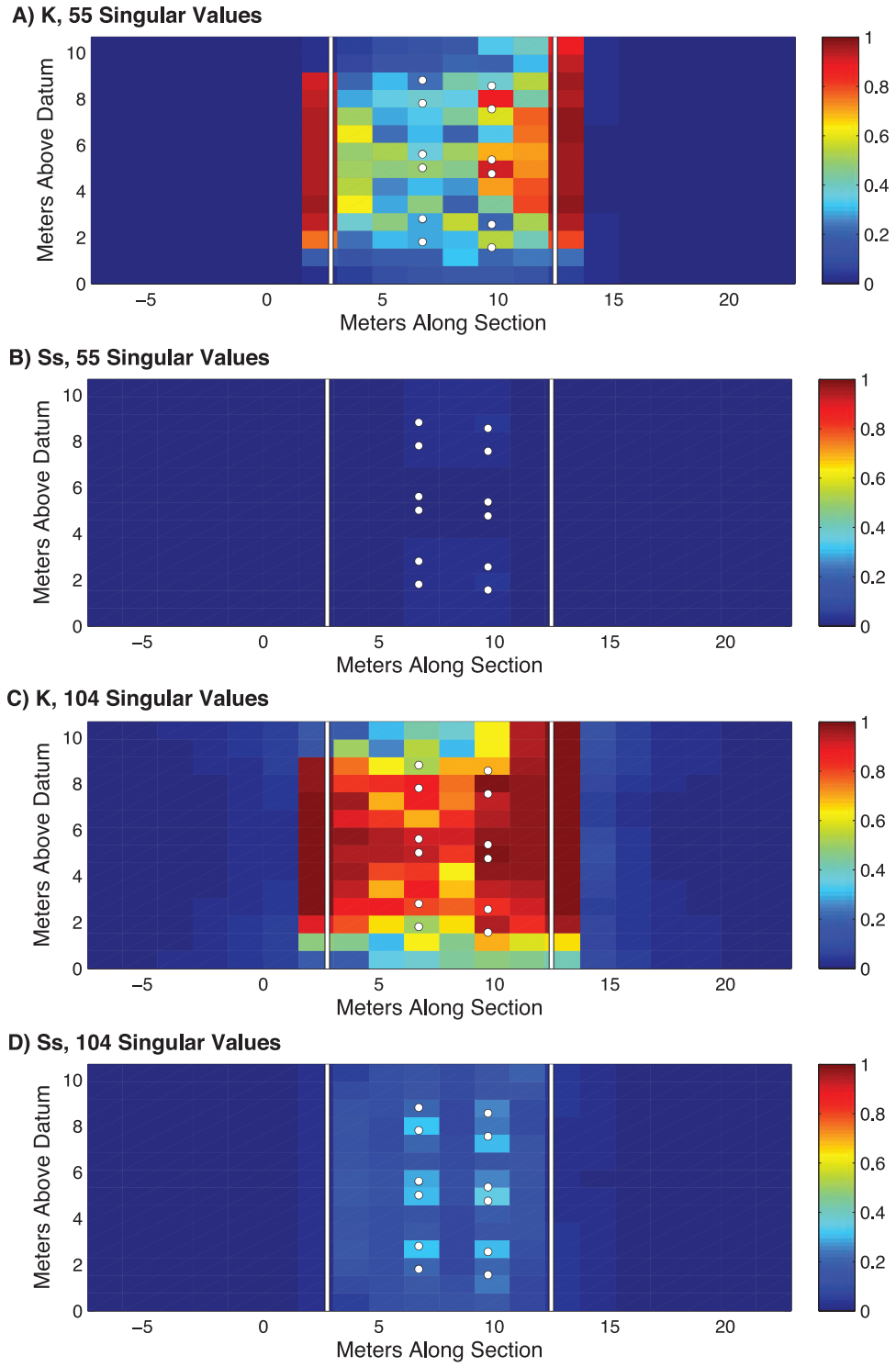

Figure 10. Diagonal elements of resolution matrix for analysis of 30-s drawdown records using truncated SVD inversion with 55 and 104 singular values: (a) K, 55 singular values, (b) S_s, 55 singular values, (c) K, 104 singular values, and (d) S_s, 104 singular values.

SVD simultaneously decomposes a matrix into both the model range and null-space, the latter representing those parameter combinations that have no (significant) influence on the model output (simulated equivalents of observed data), and the data range and null-space, the latter representing the space of data vectors (or data vector components) that have no influence on the estimated parameters, leading to nonuniqueness of the inverse solution. Increasing data correlation leads to a decrease in the amount of independent information in the data, or an increase in the effective dimension of the data null-space, but the SVD is capable of identifying the independent information in the

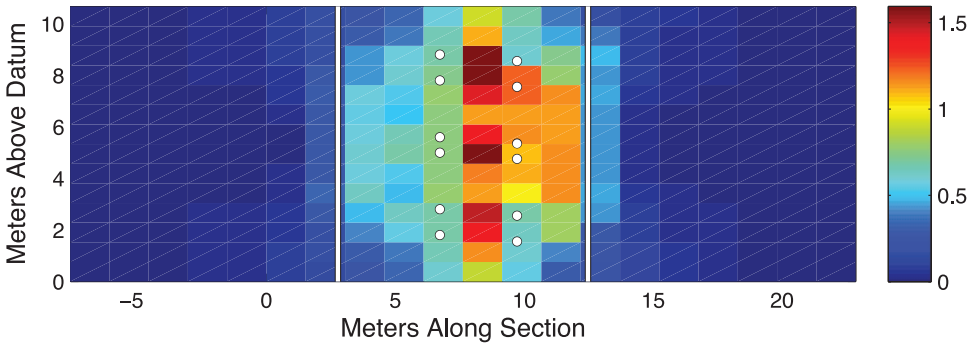

Figure 11. Root-mean-square normalized sensitivity to K for steady-shape analysis of 20–70 s data for all 23 tests.

data and using it appropriately in the estimation of the parameters.

6. Sensitivity and Resolution: Steady-Shape Analysis

[40] In this section we will examine the sensitivity and resolution associated with the steady-shape analysis of the data collected at 2-s intervals from 20 to 70 s after initiation of pumping for all 23 tests. Under steady-shape conditions, the differences in drawdown between different observation locations are identical to those that would eventually exist under true steady state conditions and thus have no dependence on specific storage, so that a steady-shape analysis focuses strictly on the estimation of K variation. Thus the sensitivity and resolution results presented here relate to the 280 K values on the Cartesian parameter grid.

[41] Using the observations from 20 to 70 s at 2-s intervals results in 26 observation times per test, with drawdowns measured at six observation ports at each time. The data values at each sample time consist of all 15 possible differences in drawdown between the distinct pairs of observation points at each observation time, resulting in 390 observed drawdown differences per test and 8970 drawdown differences over all 23 tests. We know in advance that this data set contains a high degree of redundancy, for two reasons: (1) Because we are assuming steady-shape conditions, the 26 measurements over time of the drawdown difference between a given pair of observation points should represent 26 repeat observations of essentially the same value. While actual field observations will show some variation due to any lingering transient behavior, measurement noise, and other unmodeled sources of variation, the corresponding modeled drawdown differences (those predicted by a steady state model) will all be identical. Thus, from an experimental design perspective, the repeat measurements are replicates, all corresponding to the same modeled value. In this case, inclusion of the replicate measurements allows for a clearer separation of signal from noise. (2) The 15 possible drawdown differences between the six observation ports are not all independent, since certain differences could be predicted as linear combinations of other differences. In fact, there are only five independent pieces of information among the 15 differences, meaning that all 8970 simulated drawdown differences over the 23 tests actually reduce to only 115 independent values. Nevertheless, this high degree of data redundancy is not a problem for any inverse analysis that uses a reasonable decomposition of the Jacobian matrix, such as the singular value decomposition. As discussed above, the SVD will identify the independent factors in the data (row) space of the Jacobian and use that information appropriately in the estimation of the parameters. In fact, the following analysis shows that the Jacobian in this case has an effective rank of 115, just as expected. In many inverse problems, factorization of the Jacobian matrix takes much less time than the forward model computation, so that using a data design with a high degree of redundancy should not lead to a significant increase in overall run time for the analysis. This is the case for the analysis presented here, so that we might as well use the SVD to extract the independent information in the "all possible pairs" design, alleviating the need to specify exactly which observation pairs to use.

[42] Figure 11 shows the RMS normalized sensitivity of drawdown differences over all 23 tests to the K values in the 280 parameter grid cells. This is given by

$$\sqrt{\frac{1}{n_{\Delta s}}\sum_{i=1}^{n_{\Delta s}}\left(\frac{1}{\sigma_{\Delta s}}K_j\frac{d\Delta s_i}{dK_j}\right)^2} = \sqrt{\frac{1}{n_{\Delta s}}\sum_{i=1}^{n_{\Delta s}}\left(\frac{1}{\sigma_{\Delta s}}\frac{d\Delta s_i}{d\ln K_j}\right)^2}, \tag{10}$$

where Δs_i represents a particular drawdown difference, $n_{\Delta s}$ represents the number of drawdown differences [8970] over all 23 tests, and $\sigma_{\Delta s}$ represents the standard deviation of drawdown differences, given by $\sigma_{\Delta s} = \sqrt{2\sigma_s^2} = \sqrt{2}\ \sigma_s = 2.8 \times 10^{-4}$ m. The normalization by the data standard deviation allows the sensitivity results for the transient and steady-shape cases to be compared despite the increase in expected data variance due to the use of drawdown differences rather than drawdowns themselves. Comparing Figure 11 to Figures 7a and 7c shows that the steady-shape approach focuses the sensitivity more strongly on regions between observation points, with relatively less sensitivity to the material in the immediate vicinity of the pumping wells. It is not surprising that an analysis focused on the differences between observations at different locations should be more sensitive to the material between these points. The steady-shape analysis also results in a slightly lower maximum level of RMS sensitivity relative to the expected noise level (note the difference in color scale between Figure 11 and Figures 7a and 7c), but the overall sensitivity levels are comparable in magnitude.

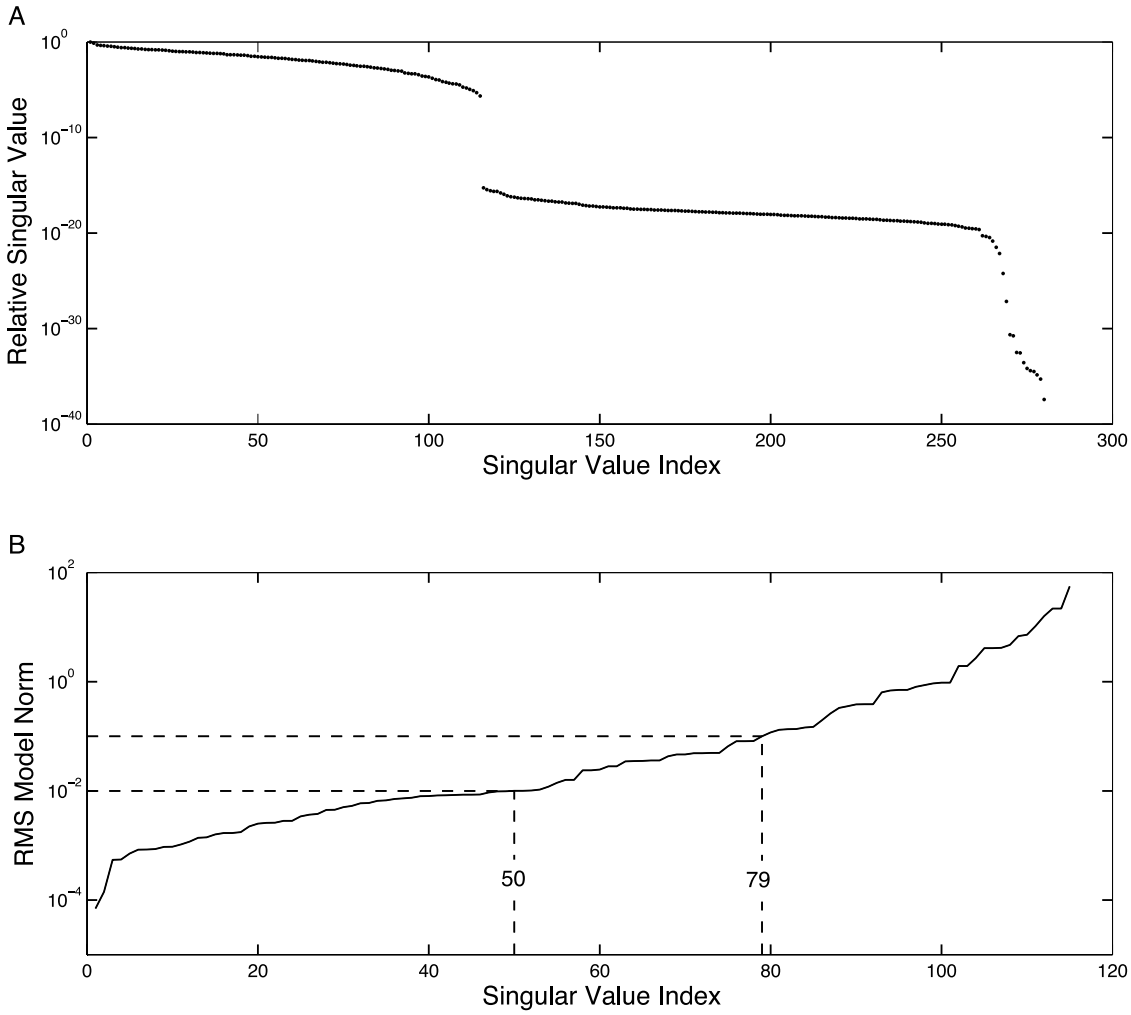

Figure 12. (a) Singular value spectrum, and (b) root-mean-square model norm associated with truncated SVD inversion of pure noise data vector for steady-shape analysis of 20–70 s data from 23 tests. Note that RMS model norm (Figure 12b) is plotted only for the first 115 of 280 singular values.

[43] Figure 12a shows the singular value spectrum for the Jacobian for the steady-shape analysis. The distinct break in the spectrum between singular value number 115 and singular value number 116 shows that the Jacobian for this problem has a rank of 115, determined by the number of independent drawdown differences over the 23 tests, as mentioned above. This means that we would not be able to estimate any more than 115 independent linear combinations of the unknown parameter ($\ln K$) values from these data, even under the most ideal conditions. In contrast, the singular value spectra for the transient analyses (Figure 8a) do not show distinct breaks, making it difficult to unambiguously identify the effective rank for these problems. Nevertheless, the effective resolution in both transient and steady-shape cases is more limited once the noise amplification behavior associated with inclusion of smaller singular values is taken into account, as demonstrated earlier for the transient analyses. Figure 12b shows the noise amplification behavior associated with the steady-shape analysis, now based on inversion of a pure noise data vector with a standard deviation of $\sigma_{\Delta s} = 2.8 \times 10^{-4}$ m. In this case, inclusion of 50 terms in the inversion leads to an RMS model norm of 1% and inclusion of 79 terms leads to a model norm of 10%. Again, these model norms can be considered as estimates of parameter error relative to a true model, with the pure noise data vector representing the residual drawdown differences relative to that model.

[44] Figure 13 shows the diagonal elements of the resolution matrix computed using the right singular vectors (columns of **V**) associated with the first 50 and first 79 singular values. Comparing Figure 13 with Figures 9 and 10 shows that the K field resolution provided by the steady-shape analysis is broadly similar to that provided by the transient analyses for comparable levels of noise amplification, although the resolution for the steady-shape analysis is more strongly focused on the regions between observation points, as we might have anticipated from the RMS sensitivity shown in Figure 11. Figure 14 presents the ratio of the steady-shape resolution (as measured by the diagonal elements of **R**) to that provided by the transient analysis of the 300-s and 30-s records for the same levels of model norm (relative parameter error). Compared with the transient analyses of the 300-s records, the steady-shape analysis provides somewhat lower resolution overall for both levels of model norm (Figures 14a and 14b). However, the ratio of the steady-shape resolution to the transient resolution is

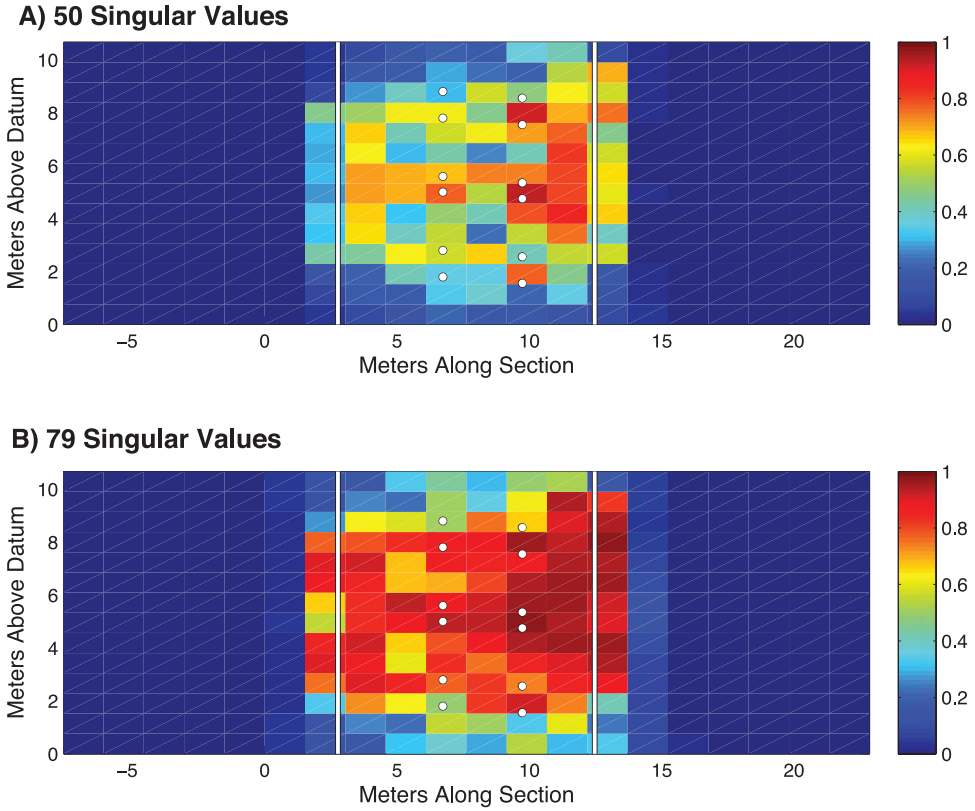

Figure 13. Diagonal elements of resolution matrix for K associated with steady-shape analysis of 20–70 s data from all 23 tests, using (a) first 50 singular values and (b) first 79 singular values.

close to 1 throughout much of the region between the wells. Ratios near 0 outside the region encompassed by the pumping wells show that the steady-shape analysis yields significantly lower resolution to variations outside the ROI, as expected, but this reduction in resolution is not really significant, since the transient analyses provided very low resolution outside the ROI to begin with (Figures 9 and 10). Figure 14c shows that for the 1% model norm case, the K field resolution for the steady-shape analysis data is higher than that for the transient analysis of the 30-s records throughout much of the region between the wells. For the 10% model norm case (Figure 14d), the ratio of resolution values is again close to 1 for much of the region between Gems4N and Gems4S, but is still greater than 1 for the most of the parameter grid cells between the observation ports.

7. Conclusions

[45] The general conclusions of this study are that (1) a steady-shape analysis of the tomographic pumping tests at GEMS is capable of providing a resolution of the K field within the region of investigation (ROI) that is comparable to that provided by a transient analysis, (2) neither approach is capable of resolving K variations outside the ROI, and (3) a transient analysis would not be able to resolve variations in S_s either inside or outside the ROI even under fairly ideal conditions where high-quality early time data could be obtained. As demonstrated in Figure 5, the drawdowns themselves remain sensitive to the bulk properties outside the ROI, both K and S_s, with the bulk K controlling the changes in drawdown over time and the bulk S_s outside the ROI acting in conjunction with the K inside the ROI to contribute a constant offset to the drawdowns (the intercept on a Cooper-Jacob plot). In contrast, after approximately 30 s, the differences in drawdown between different observation locations are controlled almost entirely by the K within the ROI. Consequently, a steady-shape analysis, based on matching these drawdown differences rather than the drawdowns themselves, tends to filter out the influence of those properties which we cannot hope to resolve even with a transient analysis, namely, K outside the ROI and S_s throughout the domain. It should be noted that these results are for an aquifer with high diffusivity (the ratio of K to S_s or T to S is of the order of 10). In lower diffusivity aquifers, the "early" time period, during which storage effects have a nonnegligible impact on changes in drawdown, will be longer, providing a greater opportunity to resolve variations in storage properties.

[46] In addition, this study has demonstrated that data redundancy in itself does not impair our ability to successfully solve an inverse problem, as long as the inversion uses a factorization algorithm that is capable of extracting the independent information in the data and using that information appropriately in constructing the estimated parameters. The work presented here is based on a singular value decomposition (SVD) of the Jacobian matrix, which serves as a linear approximation of the flow model in most groundwater inverse problems. As described by *Aster et al.* [2005], the SVD identifies which parameter combinations can be estimated from the data and which cannot (the latter forming the model null-space) and which portions of the data cannot possibly be fit by the model (the data null-

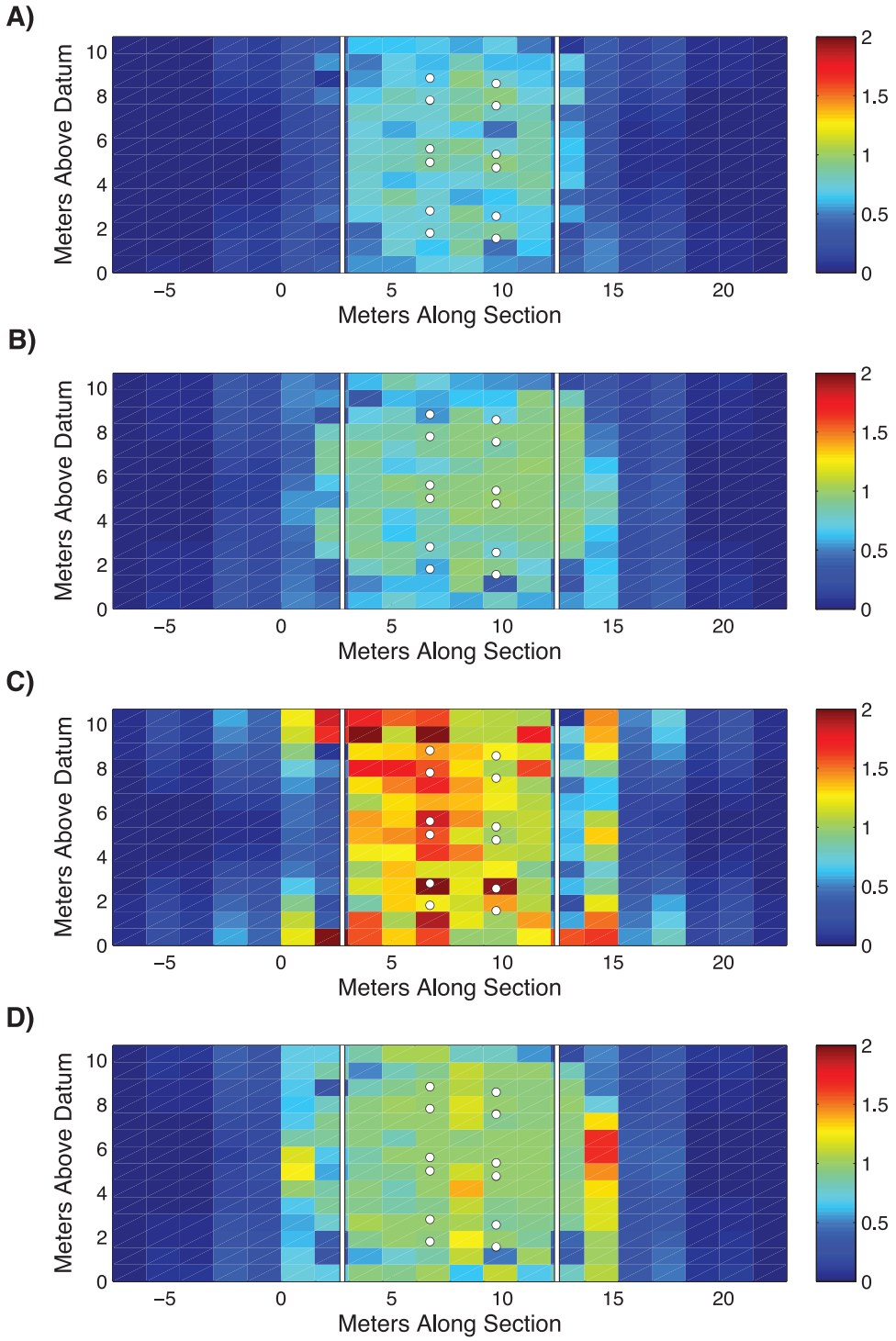

Figure 14. Resolution of steady-shape analysis of 20–70 s data relative to resolutions for transient analyses of 300- and 30-s records: (a) steady-shape with 50 singular values relative to 300-s with 84 singular values (model norm = 1%), (b) steady-shape with 79 singular values relative to 300-s with 119 singular values (model norm = 10%), (c) steady-shape with 50 singular values relative to 30-s with 55 singular values (model norm = 1%), and (d) steady-shape with 79 singular values relative to 30-s with 119 singular values (model norm = 10%).

space). In this case, the SVD of the Jacobian for the steady-shape analysis clearly identified the low data rank of this matrix resulting from the use of a highly redundant data set of drawdown differences, but this data redundancy would in no way impair the inversion process. As long as the simulation of a larger number of data (simulated equivalents of observed values) does not require significantly more run time for the forward model, as in the finite difference sensitivity approach used here or an approach based on sensitivity equations [*McElwee*, 1982; *Yeh*, 1986], an inves-

tigator might as well use a larger data set and let the matrix factorization algorithm take care of any resulting redundancy. It should be kept in mind that many geophysical survey designs intentionally incorporate a high degree of redundancy in order to increase the signal-to-noise ratio [*Telford et al.*, 1976]. In adjoint-based methods such as that described by *Zhu and Yeh* [2005], the computational burden increases with the number of observations, in which case it makes more sense to analyze to a smaller number of more independent observations. In this case, analysis of the data resolution matrix associated with a denser data record could be used to help select relatively independent observations in advance of an adjoint-based inversion [*Xia et al.*, 2008]. Like the model resolution matrix used in this study, the data resolution matrix can also be computed from the SVD of the Jacobian [*Aster et al.*, 2005].

[47] This study has investigated resolution with the parameter fields discretized at a fixed scale, using a 20×14 grid with cell dimensions 1.5 m in the horizontal direction and 0.76 m in the vertical direction. Using a finer- or coarser-scale parameter grid would of course yield somewhat different resolution results. For example, analyses with a finer grid (with cell dimensions 0.76 m horizontally and 0.3 m vertically) yielded lower resolutions per grid cell, overall. This is an unsurprising manifestation of the bias-variance tradeoff: Using a finer discretization allows for lower bias but induces higher variance and a higher degree of parameter correlation. Nevertheless, the general pattern was the same as those shown in this paper, with resolution focused on the observation points and the pumping intervals.

[48] In addition, this study has used a flow simulation model that assumes radial symmetry to investigate sensitivity to both vertical and lateral property variations in the plane encompassing the pumping and observation wells. A radially symmetric model should provide a reasonable estimate of flow behavior in this plane as long as lateral variations in the properties do not induce significant angular variations in flux toward the well, in which case the narrow angular wedge encompassing the investigated plane can be treated in isolation as a two-dimensional radial-vertical problem bounded by zero-flux boundaries in the angular direction. The first-order sensitivity analysis presented here, involving small perturbations from a homogeneous model, is not affected by significant angular variations in flux. However, the use of a radially symmetric model would have to be considered more carefully in an inverse analysis that allowed for development of significant lateral variability in the estimated parameters. Note that a radial-vertical flow model has been used here because a simple two-dimensional Cartesian model would not properly represent the radially convergent nature of the flow field.

[49] The results of this study are of course tied to the particular experimental configuration and parameter values used in the case study. These have been chosen to reflect an actual set of experiments in an alluvial aquifer. Nevertheless, the general results are in accordance with those presented by *Clemo et al.* [2003] and especially *Vasco et al.* [1997], demonstrating that pumping tests yield fairly limited resolution of the flow property variations in an aquifer, even when multiple tests with multiple observation points are analyzed simultaneously, although those studies focus on the resolution of areal property variations for vertically integrated flow, while this study focus on property variations in a vertical plane for radial-vertical flow. We can take it as a general result that even a fairly extensive sequence of hydraulic tests will provide significant resolution of flow property variations only within a certain limited distance of pumping and observation locations. In short, formulating hydraulic tests in a tomographic format does not remove the long recognized need to regularize the inverse problem by imposing an assumed model form (geostatistical or otherwise) for the spatial variability of the parameters and/or condition the estimates to auxiliary data.

[50] **Acknowledgments.** I thank Walter Illman and the two anonymous reviewers for their insightful comments on this paper. This research was supported in part by the Hydrologic Sciences Program of the National Science Foundation under grant 9903103 and the Kansas Geological Survey Applied Geohydrology Summer Research Assistantship Program. Any opinions, findings and conclusions, or recommendations expressed in this paper are those of the author and do not necessarily reflect the views of the NSF. The field efforts described herein were led by James J. Butler Jr. of the Kansas Geological Survey, with assistance provided by John Healey of the Kansas Geological Survey and Greg Davis and Sam Cain, participants in the Applied Geohydrology Summer Research Assistantship Program.

References

Aster, R. C., B. Borchers, and C. H. Thurber (2005), *Parameter Estimation and Inverse Problems*, 301 pp., Elsevier, Amsterdam.

Barrash, W., and T. Clemo (2002), Hierarchical geostatistics and multifacies systems: Boise Hydrogeophysical Research Site, Boise, Idaho, *Water Resour. Res.*, *38*(10), 1196, doi:10.1029/2002WR001436.

Barrash, W., and E. C. Reboulet (2004), Significance of porosity for stratigraphy and textural composition in subsurface, coarse fluvial deposits: Boise Hydrogeophysical Research Site, *Geol. Soc. Am. Bull.*, *9/10*, 1037–1059, doi:10.1130/B25370.1.

Boggs, J. M., S. C. Young, and L. M. Beard (1992), Field study of dispersion in a heterogeneous aquifer: 1. Overview and site description, *Water Resour. Res.*, *28*(12), 3281–3291, doi:10.1029/92WR01756.

Bohling, G. C. (1993), Hydraulic tomography in two-dimensional, steady state groundwater flow, *Eos Trans. AGU*, *74*, 141.

Bohling, G. C. (2008), Information fusion in regularized inversion of tomographic pumping tests, in *Quantitative Information for Hydrological Sciences*, *Stud. Comput. Intell.*, *79*, 137–162, Sringer, Berlin.

Bohling, G. C., and J. J. Butler Jr. (2001), Lr2dinv: A finite-difference model for inverse analysis of two-dimensional linear or radial groundwater flow, *Comput. Geosci.*, *27*(10), 1147–1156, doi:10.1016/S0098-3004(01)00036-X.

Bohling, G. C., X. Zhan, J. J. Butler Jr., and L. Zheng (2002), Steady shape analysis of tomographic pumping tests for characterization of aquifer heterogeneities, *Water Resour. Res.*, *38*(12), 1324, doi:10.1029/2001WR001176.

Bohling, G. C., J. J. Butler Jr., X. Zhan, and M. D. Knoll (2007), A field assessment of the value of steady-shape hydraulic tomography for characterization of aquifer heterogeneities, *Water Resour. Res.*, *43*, W05430, doi:10.1029/2006WR004932.

Brauchler, R., R. Liedl, and P. Dietrich (2003), A travel time based hydraulic tomographic approach, *Water Resour. Res.*, *39*(12), 1370, doi:10.1029/2003WR002262.

Butler, J. J., Jr. (1988), Pumping tests in nonuniform aquifers—he radially symmetric case, *J. Hydrol.*, *101*(1–4), 15–30.

Butler, J. J., Jr. (1990), The role of pumping tests in site characterization: Some theoretical considerations, *Ground Water*, *28*(3), 394–402, doi:10.1111/j.1745-6584.1990.tb02269.x.

Butler, J. J., Jr. (2005), Hydrogeological methods for estimation of hydraulic conductivity, edited by Y. Rubin and S. Hubbard, in *Hydrogeophysics*, pp. 23–58, Springer, New York.

Butler, J. J., Jr., and C. D. McElwee (1990), Variable-rate pumping tests for radially symmetric nonuniform aquifers, *Water Resour. Res.*, *26*(2), 291–306.

Butler, J. J., Jr., and C. D. McElwee (1995), Well-testing methodology for characterizing heterogeneities in alluvial-aquifer systems: Final technical report, *Kans. Geol. Surv. Open File*, 75–95.

Butler, J. J., Jr., and X. Zhan (2004), Hydraulic tests in highly permeable aquifers, *Water Resour. Res.*, *40*, W12402, doi:10.1029/2003WR002998.

Butler, J. J., Jr., C. D. McElwee, and G. C. Bohling (1999), Pumping tests in networks of multilevel sampling wells: Motivation and methodology, *Water Resour. Res.*, *35*(11), 3553–3560, doi:10.1029/1999WR900231.

Caers, J. (2005), *Petroleum Geostatistics*, 88 pp., Soci. of Pet. Eng., Richardson, Tex.

Carrera, J., A. Alcolea, A. Medina, J. Hidalgo, and L. J. Slooten (2005), Inverse problem in hydrogeology, *Hydrogeol. J.*, *13*, 206–222, doi:10.1007/s10040-004-0404-7.

Carrerra, J., and S. P. Neuman (1986), Estimation of aquifer parameters under transient and steady state conditions: 1. Maximum likelihood method incorporating prior information, *Water Resour. Res.*, *22*(2), 199–210, doi:10.1029/WR022i002p00199.

Clemo, T., P. Michaels, and R. M. Lehman (2003), Transmissivity resolution obtained from the inversion of transient and pseudo-steady drawdown measurements, in *Proceedings of MODFLOW and More 2003 Understanding Through Modeling*, pp. 629–633, Int. Ground Water Model. Cent., Golden Colo.

Cooper, H. H., Jr., and C. E. Jacob (1946), A generalized graphical method for evaluating formation constants and summarizing well field history, *Eos Trans. AGU*, *27*, 526–534.

Dagan, G. (1989), *Flow and Transport in Porous Formations*, 465 pp., Springer, New York.

Dagan, G., and S. P. Neuman (1997), *Subsurface Flow and Transport: A Stochastic Approach*, 241 pp., Cambridge Univ. Press, Cambridge, U.K.

Doherty, J. (2003), Ground water model calibration using pilot points and regularization, *Ground Water*, *41*(2), 170–177, doi:10.1111/j.1745-6584.2003.tb02580.x.

Driscoll, F. G. (1986), *Groundwater and Wells*, 2nd ed., 1089 pp., Johnson Div., St. Paul, Minn.

Einarson, M. D., and J. A. Cherry (2002), A new multilevel ground water monitoring system using multichannel tubing, *Ground Water Monit. Rem.*, *22*(4), 52–65, doi:10.1111/j.1745-6592.2002.tb00771.x.

Fienen, M. N., T. Clemo, and P. K. Kitanidis (2008), An interactive Bayesian geostatistical inverse protocol for hydraulic tomography, *Water Resour. Res.*, *44*, W00B01, doi:10.1029/2007WR006730.

Gelhar, L. W., and C. L. Axness (1983), Three-dimensional stochastic analysis of macrodispersion in aquifers, *Water Resour. Res.*, *19*(1), 161–180, doi:10.1029/WR019i001p00161.

Gottlieb, J., and P. Dietrich (1995), Identification of the permeability distribution in soil by hydraulic tomography, *Inverse Probl.*, *11*, 353–360, doi:10.1088/0266-5611/11/2/005.

Hastie, T., R. Tibshirani, and J. Friedman (2001), *The Elements of Statistical Learning: Data Mining, Inference, and Prediction*, 533 pp., Springer, New York.

Illman, W. A., X. Liu, and A. Craig (2007), Steady-state hydraulic tomography in a laboratory aquifer with deterministic heterogeneity: Multimethod and multiscale validation of hydraulic conductivity tomograms, *J. Hydrol.*, *341*(3–4), 222–234, doi:10.1016/j.jhydrol.2007.05.011.

Illman, W. A., A. J. Craig, and X. Liu (2008), Practical issues in imaging hydraulic conductivity through hydraulic tomography, *Ground Water*, *46*(1), 120–132, doi:10.1111/j.1745-6584.2007.00374.x.

Kitanidis, P. K. (1995), Quasi-linear geostatistical theory for inversing, *Water Resour. Res.*, *31*(10), 2411–2419, doi:10.1029/95WR01945.

Koltermann, C. E., and S. M. Gorelick (1996), Heterogeneity in sedimentary deposits: A review of structure-imitating, process-imitating, and descriptive approaches, *Water Resour. Res.*, *32*(9), 2617–2658, doi:10.1029/96WR00025.

Kruseman, G. P., and N. A. de Ridder (1990), Analysis and evaluation of pumping test data, *ILRI Publ.*, *47*, 377 pp., Int. Inst. for Land Reclam. and Impr., Wageningen, Netherlands.

Liu, S., T. -C. J. Yeh, and R. Gardiner (2002), Effectiveness of hydraulic tomography: Sandbox experiments, *Water Resour. Res.*, *38*(4), 1034, doi:10.1029/2001WR000338.

Liu, X., W. A. Illman, A. J. Craig, J. Zhu, and T.-C. J. Yeh (2007), Laboratory sandbox validation of transient hydraulic tomography, *Water Resour. Res.*, *43*, W05404, doi:10.1029/2006WR005144.

McElwee, C. D. (1982), Sensitivity analysis and the ground-water inverse problem, *Ground Water*, *20*(6), 723–735, doi:10.1111/j.1745-6584.1982.tb01392.x.

Meier, P. M., J. Carrera, and X. Sánchez-Vila (1998), An evaluation of Jacob's method for the interpretation of pumping tests in heterogeneous formations, *Water Resour. Res.*, *34*(5), 1011–1025, doi:10.1029/98WR00008.

Menke, W. (1989), *Geophysical Data Analysis: Discrete Inverse Theory*, rev. ed., 289 pp., Academic, San Diego, Calif.

Neuman, S. P. (1987), Stochastic continuum representation of fractured rock permeability as an alternative to the REV and fracture network concepts, in *Proc. U.S. Rock Mech. Symp.*, *28*, 533–561.

Rubin, Y., and S. S. Hubbard (Eds.) (2005), *Hydrogeophysics*, 523 pp., Springer, Dordrecht, Netherlands.

Rushton, K. R., and Y. K. Chan (1977), Numerical pumping test analysis in unconfined aquifers, *J. Irrig. Drain. Div. Am. Soc. Civ. Eng.*, *103*(IR1), 1–12.

Sánchez-Vila, X., P. M. Meier, and J. Carrera (1999), Pumping tests in heterogeneous aquifers: An analytical study of what can be obtained from their interpretation using Jacob's method, *Water Resour. Res.*, *35*(4), 943–952, doi:10.1029/1999WR900007.

Settari, A., and K. Aziz (1974), A computer model for two-phase coning simulation, *SPE J.*, *14*(3), 221–236.

Straface, S., T.-C. J. Yeh, J. Zhu, S. Troisi, and C. H. Lee (2007), Sequential aquifer tests at a well field, Montalto Uffugo Scalo, Italy, *Water Resour. Res.*, *43*, W07432, doi:10.1029/2006WR005287.

Sudicky, E. A. (1986), A natural gradient experiment on solute transport in a sand aquifer: Spatial variability of hydraulic conductivity and its role in the dispersion process, *Water Resour. Res.*, *22*(13), 2069–2082, doi:10.1029/WR022i013p02069.

Sun, N.-Z. (1994), *Inverse Problems in Groundwater Modeling*, 337 pp., Kluwer Acad, Dordrecht, Netherlands.

Telford, W. M., L. P. Geldart, R. E. Sheriff, and D. A. Keys (1976), *Applied Geophysics*, 860 pp., Cambridge Univ. Press, New York.

Tonkin, M. J., and J. Doherty (2005), A hybrid regularization methodology for highly parameterized environmental models, *Water Resour. Res.*, *41*, W10412, doi:10.1029/2005WR003995.

Tosaka, H., K. Masumoto, and K. Kojima (1993), Hydropulse tomography for identifying 3-D permeability distribution, in *High Level Radioactive Waste Management: Proceedings of the Fourth Annual International Conference of the ASCE*, pp. 955–959, Am. Soc. Civ. Eng., Reston, Va.

Vasco, D. W., A. Datta-Gupta, and J. C. S. Long (1997), Resolution and uncertainty in hydrologic characterization, *Water Resour. Res.*, *33*(3), 379–397, doi:10.1029/96WR03301.

Vesselinov, V. V., S. P. Neuman, and W. A. Illman (2001a), Three-dimensional numerical inversion of pneumatic cross-hole tests in unsaturated fractured tuff: 1. Methodology and borehole effects, *Water Resour. Res.*, *37*(12), 3001–3017, doi:10.1029/2000WR000133.

Vesselinov, V. V., S. P. Neuman, and W. A. Illman (2001b), Three-dimensional numerical inversion of pneumatic cross-hole tests in unsaturated fractured tuff: 2. Equivalent parameters, high-resolution stochastic imaging, and scale effects, *Water Resour. Res.*, *37*(12), 3019–3041, doi:10.1029/2000WR000135.

Vogel, C. R. (2002), *Computational Methods for Inverse Problems*, 183 pp., Soc. for Ind. and Appl. Math., Philadelphia, Pa.

Xia, J., R. D. Miller, and Y. Xu (2008), Data-resolution matrix and model-resolution matrix for Rayleigh-wave inversion using a damped least-squares method, *Pure Appl. Geophys.*, *165*, 1227–1248, doi:10.1007/s00024-008-0364-2.

Yeh, T.-C. J., and S. Liu (2000), Hydraulic tomography: Development of a new aquifer test method, *Water Resour. Res.*, *36*(8), 2095–2105, doi:10.1029/2000WR900114.

Yeh, W. W.-G. (1986), of parameter identification procedures in groundwater hydrology: The inverse problem, *Water Resour. Res.*, *22*(2), 95–108, doi:10.1029/WR022i002p00095.

Zemansky, G. M., and C. D. McElwee (2005), High-resolution slug testing, *Ground Water*, *43*(2), 222–230, doi:10.1111/j.1745-6584.2005.0008.x.

Zheng, C., and S. M. Gorelick (2003), Analysis of solute transport in flow fields influenced by preferential flow paths at the decimeter scale, *Ground Water*, *41*(2), 142–155, doi:10.1111/j.1745-6584.2003.tb02578.x.

Zhu, J., and T.-C. J. Yeh (2005), Characterization of aquifer heterogeneity using transient hydraulic tomography, *Water Resour. Res.*, *41*, W07028, doi:10.1029/2004WR003790.

G. C. Bohling, Kansas Geological Survey, University of Kansas, 1930 Constant Avenue, Lawrence, KS 66047, USA. (geoff@kgs.ku.edu)